

Low-frequency two-dimensional linear instability of plane detonation

By MARK SHORT¹† AND D. SCOTT STEWART²

¹ School of Mathematics, University of Bristol, Bristol BS8 1TW, UK

² Theoretical and Applied Mechanics, University of Illinois, Urbana, IL 61801, USA

(Received 27 March 1996 and in revised form 22 November 1996)

An analytical dispersion relation describing the linear stability of a plane detonation wave to low-frequency two-dimensional disturbances with arbitrary wavenumbers is derived using a normal mode approach and a combination of high activation energy and Newtonian limit asymptotics, where the ratio of specific heats $\gamma \rightarrow 1$. The reaction chemistry is characterized by one-step Arrhenius kinetics. The analysis assumes a large activation energy in the plane steady-state detonation wave and a characteristic linear disturbance wavelength which is longer than the fire-zone thickness. Newtonian limit asymptotics are employed to obtain a complete analytical description of the disturbance behaviour in the induction zone of the detonation wave. The analytical dispersion relation that is derived depends on the activation energy and exhibits favourable agreement with numerical solutions of the full linear stability problem for low-frequency one- and two-dimensional disturbances, even when the activation energy is only moderate. Moreover, the dispersion relation retains vitally important characteristics of the full problem such as the one-dimensional stability of the detonation wave to low-frequency disturbances for decreasing activation energies or increasing overdrives. When two-dimensional oscillatory disturbances are considered, the analytical dispersion relation predicts a monotonic increase in the disturbance growth rate with increasing wavenumber, until a maximum growth rate is reached at a finite wavenumber. Subsequently the growth rate decays with further increases in wavenumber until the detonation becomes stable to the two-dimensional disturbance. In addition, through a new detailed analysis of the behaviour of the perturbations near the fire front, the present analysis is found to be equally valid for detonation waves travelling at the Chapman–Jouguet velocity and for detonation waves which are overdriven. It is found that in contrast to the standard imposition of a radiation or piston condition on acoustic disturbances in the equilibrium zone for overdriven waves, a compatibility condition on the perturbation jump conditions across the fire zone must be satisfied for detonation waves propagating at the Chapman–Jouguet detonation velocity. An insight into the physical mechanisms of the one- and two-dimensional linear instability is also gained, and is found to involve an intricate coupling of acoustic and entropy wave propagation within the detonation wave.

† Present address: Theoretical and Applied Mechanics, University of Illinois, Urbana, IL 61801, USA.

1. Introduction

1.1. *The multi-dimensional detonation instability problem*

It has been established, both experimentally and theoretically, that plane steady gaseous detonation waves are inherently unstable. Pulsating bow shock detonation instabilities with a one-dimensional character have been observed off the forward surface of hypersonic spherical projectiles travelling in an explosive atmosphere (Alpert & Toong 1972). Similarly, numerical simulations of strictly one-dimensional detonation waves for a standard model with a one-step Arrhenius reaction rate exhibit longitudinal pulsating instabilities (Fickett & Wood 1966; Abouseif & Toong 1982; Bourlioux, Majda & Roytburd 1991; Quirk 1994). In contrast, two-dimensional unstable detonation waves display a prominent cellular instability that has a different character to the pulsating one-dimensional instability. Experiments in gases show that cellular detonation has a complex multi-dimensional structure, with transverse shock waves propagating along the face of the lead shock (Strehlow 1970).

A model of detonation, defined by the reactive Euler equations with an ideal equation of state and a single exothermic reaction with Arrhenius kinetics, was used by Erpenbeck (1964) to study the stability of plane detonations. Subsequently, this model has become the paradigm for analytical and numerical studies of detonation stability and dynamics in terms of the parameters that define the steady state, such as the ratio of specific heats, the heat of combustion, the activation energy and steady detonation speed. The steady plane detonation structure of the standard model is the Zeldovich–von Neumann–Döring wave, which is obtained by using the first integrals of mass, momentum and energy conservation in the reaction zone to substitute for the reaction progress variable in the rate equation. This in turn is solved for the spatial distribution of fuel (say) in the reaction zone.

1.2. *One-dimensional low-frequency instability*

The system of ordinary differential equations governing the stability of linear normal mode disturbances of the steady solutions has non-constant coefficients due to the spatial variation of the steady state (Lee & Stewart 1990). For the general case, an exact analytical solution of the linear stability equations is not practically possible. Instead, a numerical treatment is required. The normal mode formulation and approach proposed in Lee & Stewart (1990) solves the stability equations numerically and provides a straightforward means to obtain exact solutions to the stability problem for the standard model. Subsequently, the normal mode formulation was used by Short (1997) to study the bifurcation behaviour of the one-dimensional linear stability spectrum as the activation energy is increased into regimes where previous large-activation-energy studies might reasonably be expected to apply. Of most interest, for reasons which are apparent from the numerical simulations described below, is the behaviour of the lowest-frequency mode.

Typically, for moderate activation energies, there is a single oscillatory low-frequency mode present in the one-dimensional linear stability spectrum, in addition to several other modes with larger growth rates and frequencies (Lee & Stewart 1990; Short 1997). When the activation energy is increased, the period of the lowest-frequency mode increases until a critical activation energy is reached at which this low-frequency oscillatory mode bifurcates into two non-oscillatory modes (Short 1997). The growth rate of one of the non-oscillatory modes then decays with further increases in the activation energy, and corresponds to the low-frequency non-oscillatory mode identified analytically by Buckmaster & Ludford (1987). Short (1997) also

finds that for very large activation energies, the one-dimensional stability spectrum consists of a very large number of unstable modes whose growth rates increase with increasing frequency. One of the major objections in the past to use of the classical square-wave model (Erpenbeck 1963) to study detonation instability is the so-called pathological instability spectrum, in which there is an infinite number of unstable modes whose growth rates increase with increasing frequency. However, the work of Short (1997) has shown numerically that such behaviour is an actual feature of the standard detonation model in the limit of infinite activation energies.

The particular interest in the behaviour of the lowest-frequency linear mode stems from numerical studies of one-dimensional pulsating detonation wave propagation (Abouseif & Toong 1982; Bourlioux *et al.* 1991; Quirk 1994). For steady detonation flows with parameters near those that define the linear neutral stability boundary, the pulsation period of the nonlinear oscillation agrees almost identically with the period of the lowest-frequency mode present in the linear stability spectrum, even for very long propagation times of the unstable detonation. This agreement between the two periods is maintained even as the steady detonation parameters are varied substantially away from those corresponding to neutral stability towards greater instability. In contrast, although excited initially, the higher-frequency linearly unstable modes are observed to erode rapidly, leading to the conclusion that the high-frequency unstable linear modes are nonlinearly stable. Thus even in the presence of several linearly unstable modes with larger growth rates, the lowest-frequency mode appears to determine the period of the nonlinear pulsation of the unstable one-dimensional detonation wave; an accurate analytical representation of the high-frequency modes is therefore not required to describe the detonation dynamics. Indeed Abouseif & Toong (1982) made similar observations, and probably were the first to suggest that even for unstable detonations, the properties of the low-frequency linear spectra of unstable one-dimensional detonation waves could be used to predict the salient features of the acoustic mechanism of the low-frequency nonlinear pulsation.

1.3. Two-dimensional low-frequency instability

In contrast to the significant advances made in one-dimensional computations, accurate numerical simulation of two-dimensional detonation wave propagation is severely hampered by the extremely fine spatial and temporal scales which characterize the intricate hydrodynamical and chemical coupling in multi-dimensional flow. Advances in two-dimensional computations for the standard detonation model have, however, been made, most notably by Bourlioux & Majda (1992) and Quirk (1994, 1995). The latter involves the use of sophisticated adaptive mesh refinement techniques. However, even with the mesh refinement, it is not clear that a spatially resolved and wholly converged representation of two-dimensional cellular detonation has ever been carried out. Thus conclusions concerning two-dimensional detonation dynamics obtained from direct numerical simulation, in particular those regarding the detonation cell spacing, should be regarded as tentative.

Recently, Short (1997) has conducted a numerical investigation into the two-dimensional linear stability of plane detonations using a normal mode formulation. Typically, it is found that for moderate activation energies, the growth rate of each unstable one-dimensional oscillatory mode, whether low frequency or high frequency, increases monotonically with increasing wavenumber until a maximum growth rate is reached at a finite wavenumber. Subsequently, the growth rate of each mode decays with further increases in wavenumber until each mode ultimately becomes stable at a sufficiently large wavenumber. Moreover there is a series of modes which, despite

being one-dimensionally stable, is found to be unstable for finite bands of wavenumbers. So in general, there is a series of unstable modes with maximum growth rates at well-defined wavenumbers, and a unique wavenumber above which the detonation is stable to all two-dimensional disturbances. According to classical hydrodynamic stability theory, one would predict that the wavenumber corresponding to the maximum growth rate, regardless of the corresponding frequency, will determine the detonation cell spacing observed (see Bourlioux & Majda 1992 for further discussions). However by analogy with the one-dimensional behaviour, there is reason to suspect that in the early stages of cell formation, the wavenumber associated with the maximum growth rate of the lowest-frequency unstable two-dimensional mode will offer a substantially better comparison. Calculations by Quirk (personal communication, 1995) appear to support this conjecture.

With this in mind, Short (1997) has made detailed studies of the behaviour of the lowest-frequency two-dimensionally unstable mode for a range of values of the activation energy and detonation overdrive. When a single one-dimensional oscillatory low-frequency mode is present, the stability behaviour of the mode is as described above. On the other hand, for sufficiently large activation energies, there are two non-oscillatory one-dimensional modes. It is found that as the wavenumber is increased, there is a critical wavenumber at which the two non-oscillatory modes merge into a single oscillatory mode. Subsequently the growth rate of this oscillatory mode can either increase with further increases in the wavenumber, reach a maximum and then decay to a stable mode, or it can decay monotonically until stability is attained. In such cases, it is difficult to select a cell-spacing based on the wavenumber corresponding to the maximum growth rate, since this is the one-dimensional unstable mode. Thus, the problem faced is to determine how all the different types of low-frequency linear stability behaviour can relate to a nonlinear detonation cell spacing. Solutions to this problem are discussed later in the paper.

In summary, there is a significant amount of evidence that in both one- and two-dimensional problems, there is a range of detonation parameters where a definitive link exists between the low-frequency portions of the unstable linear spectra and the nonlinear mechanisms of detonation instability. Thus an analytically tractable theory of the low-frequency linear instability of the plane steady detonation wave is desired.

1.4. Previous asymptotic approaches

Rational asymptotic approaches to the linear stability problem for the standard model are limited in number, and thus far mainly appear in the works of Erpenbeck (1963), Buckmaster & Ludford (1987), Buckmaster & Neves (1988), Buckmaster (1989), Yao & Stewart (1996) and Short (1996). All of the work mentioned involves the limit of a large activation energy, where the steady detonation wave assumes the well-known square-wave structure. The shock ignites the material and is followed by an induction zone of small reaction depletion. The induction zone has a well-defined length \tilde{L}^* , and is followed by a thin reaction zone commonly referred to as the 'fire'. The fire zone is connected to a trailing, effectively inert-equilibrium (or burnt) zone (figure 1).

In one of the first modern uses of activation energy asymptotics, Erpenbeck (1963) presented the first rational investigation of the linear stability of detonation in the limit of large activation, using a Laplace transform formulation. It was demonstrated that the Zaidel (1961) *ad-hoc* stability model, in which the steady-state detonation structure is replaced by a piecewise-constant structure, possesses an infinite number of unstable modes whose growth rates increase with increasing frequency. Using a formal asymptotic analysis and a normal mode formulation, Buckmaster & Neves (1988)

considered the behaviour of one-dimensional disturbances in the limit of large activation energy, where the disturbance frequency and growth rate were assumed to be $O(1)$ on the time scale of acoustic passage across the induction zone $\tilde{L}^*/\tilde{c}_s^*$, \tilde{c}_s^* being the adiabatic post-shock sound speed. Buckmaster & Neves (1988) found that the linear stability spectrum consisted of an infinite number of unstable oscillatory modes, whose growth rates increased monotonically with increasing frequency. This thus demonstrated that the spectrum determined by Erpenbeck (1963) is in fact representative of the linear stability spectrum in the limit of large activation energies, as verified numerically by Short (1997).

Buckmaster & Ludford (1987) is concerned with two-dimensional slowly varying small-wavenumber disturbances. Specifically, the disturbances are taken to evolve on the time scale $\theta\tilde{L}^*/\tilde{c}_s^*$, where θ represents the non-dimensional large activation energy. The transverse disturbances are assumed to have a characteristic wavelength $\theta\tilde{L}^*$. They found a single non-oscillatory eigenvalue whose growth rate increased with increasing wavenumber. Buckmaster (1989) later extended the analysis of Buckmaster & Ludford (1987) to transverse disturbances which have a characteristic wavelength $O(\theta^{1/2}\tilde{L}^*)$, and again found a single non-oscillatory unstable eigenvalue, but with growth rates which decrease as the wavenumber increases. Buckmaster (1989) was then able to deduce an intermediate wavelength scaling, namely $O(\theta^{2/3}\tilde{L}^*)$, at which a maximum growth rate is obtained, and suggested that this scaling could correspond to a nonlinear detonation cell spacing.

Using both a sequential limit and a distinguished limit between the inverse activation energy θ^{-1} and $(\gamma - 1)$, where γ is the ratio of specific heats, Short (1996) has investigated the two-dimensional stability of the square-wave detonation. As in Buckmaster & Neves (1988), the evolution time of the disturbances is explicitly scaled with respect to the steady detonation induction time. Under a sequential limit between $(\gamma - 1)$ and θ^{-1} , where $(\gamma - 1) \gg \theta^{-1}$, the dispersion relation is obtained by a compatibility condition on the flame front perturbation, and confines the stability problem to an analysis of the induction zone only. For the one-dimensional problem, an infinite number of unstable modes are again found, whose growth rates increase with increasing frequency. Moreover, the asymptotic dispersion relation derived in Short (1996) reproduces the numerical results of Buckmaster & Neves (1988) almost identically.

Having conducted this asymptotic analysis, further observations on the presence of an infinite number of oscillatory modes in both the studies of Buckmaster & Neves (1988) and Short (1996) can be made. We conclude that this feature is not a failure of the detonation model, as shown numerically by Short (1997), but rather for large but finite activation energies it represents a breakdown of asymptotic expansions in the high-frequency range of the spectrum. In both these studies, frequencies are explicitly assumed to be larger than the fire-zone thickness. For high frequencies and finite but large activation energies, a rescaling of the characteristic disturbance parameters would be required to describe the high-frequency portions of the stability spectrum, taking into account the exponentially large frequencies which would affect the quasi-steady fire-zone structure. Such an asymptotic study should verify the known numerical result that sufficiently large-frequency disturbances are stable (Lee & Stewart 1990). When two-dimensional disturbances are considered in the sequential limit studied in Short (1996), it is found that the growth rate of each one-dimensionally unstable mode decays monotonically with increasing wavenumber, until a critical wavenumber is reached at which each mode becomes stable.

When a distinguished limit between θ^{-1} and $(\gamma - 1)$ is considered, where $(\gamma - 1) =$

$O(\theta^{-1})$, Short (1996) demonstrates that the dispersion relation is found by calculating an induction-zone solution, and matching this solution across the flame front to an acoustic radiation condition in the equilibrium zone. For the one-dimensional problem an infinite number of unstable modes are again found, whose growth rates increase with increasing frequency. However when transverse disturbances are considered in the distinguished limit, the growth rate of each one-dimensionally unstable mode first increases with increasing wavenumber, before reaching a maximum growth rate at a critical finite wavenumber. The growth rate of each mode then decays monotonically with increasing wavenumber, until a wavenumber is reached at which stability prevails. Thus the stability behaviour found by considering a distinguished limit between θ^{-1} and $(\gamma - 1)$ agrees qualitatively with the behaviour predicted by an exact numerical solution of the linear spectrum (Short 1997) for sufficiently large activation energies. Based on the idea proposed above, namely that the maximum growth of the lowest-frequency mode corresponds to an initial cell sizing, the asymptotic theory developed by Short (1996) thus provides an estimate of the expected initial cell sizing in the limit of large activation energy.

1.5. Nonlinear detonation cell spacing

Despite the conjectures which can be made about cell spacing based solely upon linear stability theory, a definitive criterion can ultimately only be obtained from an analytical nonlinear theory. Recently, using combined limits of near Chapman–Jouguet detonation velocity, large dimensionless activation energy and slow dynamic shock evolution measured on the time scale of particle passage through the reaction zone, Yao & Stewart (1996) have systematically derived a two-dimensional intrinsic evolution equation for the motion of the lead detonation shock front. Their evolution equation is a partial differential equation in the shock displacement, and is a relation between the normal shock velocity, the first and second time derivatives of the normal shock velocity, the shock curvature, and the first normal time derivative of the shock curvature. The equation is third order in time and second order in space.

When the equation is solved numerically, large detonation cells with a unique spacing substantially longer than the steady induction-zone length are found to emerge after a long propagation time, even though the linear stability spectrum corresponding to the evolution equation does not have a local maximum growth rate. Smaller cells, which appear initially, tend to be absorbed by the larger cells during their nonlinear interaction. The wavelength of the final cell spacing is found to correspond with the point of linear neutral stability in wavenumber space. For the range of parameters in which the Yao & Stewart (1996) analysis predicts cells, this point also corresponds to the point of maximum phase velocity and group velocity for the low-frequency mode. Thus, although the Yao & Stewart (1996) analysis only predicts cells for a restrictive range of linear dispersion relations, it does raise the possibility that a criterion for determining the cell spacing in more general cases could be based on the wavelength at which the maximum group velocity occurs in the linear stability spectrum. Typically, as shown later, such wavelengths are substantially larger than the steady induction-zone length, the main feature of cell spacing which is observed experimentally (Strehlow 1970).

1.6. Present approach

The main drawback with the previous high-activation-energy approaches is that activation energy scalings have been *a priori* attached to explicit algebraic expansions in the activation energy for the disturbance growth rates, frequencies and wavenumbers.

This leads to dispersion relations that have a narrow range of validity. Thus, in the present analysis we have been led to pursue rational asymptotic limits of the exact linear stability problem for the standard model in limits suitable for gaseous detonation, to make improvements on and remove the deficiencies of some of the previous work in this direction. In our present work, we use an asymptotic strategy based on that used in Short (1996) that uses the limit of large activation energy to generate a limiting form of the stability problem that reflects the square-wave structure, but we do not attach *a priori* expansions for the disturbance characteristics. The general asymptotic problem is then solved analytically, as opposed to numerically, by using the limit $\gamma \rightarrow 1$, in which solutions are obtained explicitly to $O(\gamma - 1)$.

The analysis proceeds as follows. First we derive the exact two-dimensional linear stability problem in its most general form without asymptotic simplification. The steady detonation state is expressed in its limiting form for large activation energy, consisting of a well-defined induction zone, thin fire zone and equilibrium zone structure. A stability problem for linear disturbances in the induction zone is then derived, in which terms which are explicitly $O(1/\theta)$ relative to the retained terms are omitted. Note that no assumptions regarding the growth rates, frequencies or wavenumbers of the disturbance are made at this stage. The linear stability problem in the induction zone is then solved in the limit $\gamma \rightarrow 1$, where the heat of combustion is assumed to be inversely proportional to $(\gamma - 1)$, so that the product of the heat of combustion time and the heat release is $O(1)$. This limit ensures that we are far away from a small-heat-release limit.

We then derive a dispersion relation for all disturbances which have a characteristic wavelength larger than the exponentially thin fire zone (which we define as *low-frequency*). The linearized shock relations are connected via an analytical solution of the induction zone to the fire. The fire location is determined so that an apparent singularity in the induction-zone expansion is suppressed. This is achieved through a Poincaré–Kuo–Lighthill straining of the induction-zone coordinate. Since we confine our present investigations to low-frequency disturbances, the fire can be represented as a discontinuous Rankine–Hugoniot deflagration by its jump relations, which connect the solution ahead of the fire to that behind. Finally a radiation condition is applied in the burnt or equilibrium zone, providing the extra homogeneous condition required to specify the dispersion relation. Also, as well as deriving an analytical dispersion relation for overdriven detonation waves, a rational derivation of an analytical dispersion relation corresponding to Chapman–Jouguet detonation waves is given. We then show comparisons of our asymptotically derived results with numerical results for the exact spectra. Even for moderate activation energies, the comparison between the exact and asymptotic predictions is very favourable in both one and two dimensions and for all detonation speeds.

Our work also includes the important resolution of any remaining concerns regarding the ill-posed nature of the linear stability of the Chapman–Jouguet detonation wave. This is achieved through a detailed analysis of the jump conditions across the Rankine–Hugoniot discontinuity and the nature of the perturbation behaviour in the burnt gas. For overdriven detonation waves, where the steady flow in the burnt gas is subsonic, the standard condition that specifies the dispersion relation is an acoustic radiation condition which prevents upstream propagation of disturbances from infinity. However, this choice is not unique in determining the burnt gas behaviour. For the Chapman–Jouguet detonation wave, where the steady flow in the burnt gas is exactly sonic, we find that an acoustic radiation condition *must* be satisfied, and since there is no choice in the behaviour of the burnt-zone conditions, the general

perturbation jump conditions across the flame front are then degenerate. This leads to a compatibility condition on the jump conditions across the fire zone in order to determine the dispersion relation for Chapman–Jouguet waves.

The remainder of the paper is as follows. In §2 we describe the model equations and reaction rate law. In §3 we describe the detonation structure in the limit of large activation energy. Section 4 states the exact linear stability problem. The approximation to the exact stability problem in the limit of large activation energy is stated in the induction zone, and is solved analytically by use of the Newtonian limit, where $\gamma \rightarrow 1$. The Rankine–Hugoniot relations for the fire-front perturbations are given and the acoustic properties of the equilibrium zone are discussed. The asymptotic forms of the dispersion relation for both overdriven waves and Chapman–Jouguet waves are derived in §4. Section 5 discusses the mechanism of detonation instability as determined from the analytical analysis, and predictions of the asymptotically derived dispersion relation are compared with numerical calculations of the exact stability problem in §6.

2. Model

The equations describing the hydrodynamic evolution of a detonation wave are the reactive Euler equations

$$\left. \begin{aligned} \frac{D\rho}{Dt} + \rho \nabla \cdot \mathbf{u} &= 0, & \rho \frac{D\mathbf{u}}{Dt} &= -\nabla p, & \frac{De}{Dt} + p \frac{D\rho^{-1}}{Dt} &= 0, \\ \frac{DY}{Dt} &= r, & r &= r(p, \rho, Y), & e &= e(p, \rho, Y), \end{aligned} \right\} \quad (2.1)$$

for density ρ , velocity \mathbf{u} , pressure p and reactant mass fraction Y . Here $Y = 1$ represents unreacted material while $Y = 0$ represents completely burnt material. The specific internal energy e and equation of state are taken to correspond to an ideal perfect gas, such that

$$e = \frac{p}{(\gamma - 1)\rho} + QY, \quad RT = \frac{p}{\rho}, \quad (2.2)$$

for temperature T , ratio of specific heats γ , chemical heat release factor Q and gas constant R . The rate law r is taken to be the one-step irreversible Arrhenius reaction

$$r = -KY \exp\left(-\frac{E}{RT}\right), \quad (2.3)$$

where K is the Arrhenius pre-exponential factor and E is the activation energy of the reaction. Non-dimensional scales are chosen with reference to the one-dimensional steady detonation wave. In particular the density, temperature and velocity scales are the detonation shock density $\tilde{\rho}_s^*$, temperature \tilde{T}_s^* and sound speed \tilde{c}_s^* respectively. Here, and subsequently, we adopt the notation of a tilde to refer to dimensional quantities, an asterisk to represent steady values, and the subscript s to correspond to the detonation shock values. The scaling of pressure is taken with respect to $\tilde{\rho}_s^* \tilde{c}_s^{*2}$, while the characteristic length scale \tilde{L}^* is chosen as

$$\tilde{L}^* = \left(\frac{\tilde{c}_s^*}{\tilde{K}}\right) \frac{\mathcal{K} e^\theta}{\beta \theta}, \quad (2.4)$$

which is the steady induction-zone length in the limit of large activation energy (Buckmaster & Ludford 1987). The non-dimensional activation energy θ and heat

release β appearing in (2.4) are defined by

$$\theta = \frac{\tilde{E}}{\tilde{R}\tilde{T}_s^*}, \quad \beta = \frac{(\gamma - 1)\tilde{Q}}{\tilde{c}_s^{*2}}, \quad (2.5)$$

while the constant \mathcal{K} is given by

$$\mathcal{K} = \frac{M_s(M_s^2 - 1)}{\gamma M_s^2 - 1}, \quad (2.6)$$

where M_s is the steady post-shock particle Mach number defined as

$$M_s = \frac{\tilde{u}_s^*}{\tilde{c}_s^*}, \quad (2.7)$$

and u_s^* is the dimensional post-shock particle velocity. It is also useful at this stage to define Erpenbeck's (1964) alternative definitions for the activation energy and heat release, which do not depend on the shock speed. These are

$$Q = \frac{\gamma\tilde{Q}}{\tilde{c}_0^{*2}}, \quad E = \frac{\gamma\tilde{E}}{\tilde{c}_0^{*2}}, \quad (2.8)$$

where \tilde{c}_0^* is the pre-shock sound speed. The relationships between θ and E and β and Q are given by

$$\beta = \frac{\gamma - 1}{\gamma} \frac{Q}{\tilde{c}_s^{*2}/\tilde{c}_0^{*2}}, \quad \theta = \frac{E}{\tilde{c}_s^{*2}/\tilde{c}_0^{*2}}, \quad (2.9)$$

where

$$\frac{\tilde{c}_s^{*2}}{\tilde{c}_0^{*2}} = \frac{(2\gamma D^2 - \gamma + 1)(2 + (\gamma - 1)D^2)}{(\gamma + 1)^2 D^2}, \quad (2.10)$$

and $D = \tilde{D}/\tilde{c}_0^*$ is the propagation Mach number of the steady one-dimensional detonation relative to the upstream pre-shock reactive atmosphere. Finally, the time scale is given by $\tilde{L}^*/\tilde{c}_s^*$. With these scalings, the equations (2.1)–(2.3) can be written in the non-dimensional form

$$\left. \begin{aligned} \frac{D\rho}{Dt} + \rho\nabla \cdot \mathbf{u} &= 0, & \rho \frac{D\mathbf{u}}{Dt} &= -\nabla p, & \rho \frac{DT}{Dt} &= (\gamma - 1) \frac{Dp}{Dt} - \beta\rho \frac{DY}{Dt}, \\ \frac{DY}{Dt} &= r = -\frac{\mathcal{K}}{\theta\beta} Y \exp\left[\theta\left(1 - \frac{1}{T}\right)\right], & T &= \gamma p/\rho, \end{aligned} \right\} \quad (2.11)$$

where the convective derivative D/Dt is given by

$$\frac{D}{Dt} = \frac{\partial}{\partial t} + u \frac{\partial}{\partial n} + v \frac{\partial}{\partial y}, \quad (2.12)$$

for a horizontal velocity component u and horizontal Cartesian coordinate n that are both in a frame of reference attached to the steady detonation shock, and a transverse velocity component and transverse Cartesian coordinate given by v and y respectively.

Below, we will assume the following asymptotic ordering for θ and β :

$$\theta \gg 1, \quad \beta \sim O(1). \quad (2.13)$$

The scaling of the heat release factor β is chosen such that in the asymptotic limit where the specific heats ratio $\gamma \rightarrow 1$, we maintain a strong leading-order coupling

between chemical and gasdynamic evolutions. It is emphasized that we are not concerned with a weak heat release limit.

3. Steady detonation structure

For a Mach number D relative to the upstream uniform reactive atmosphere, the overdrive f_{OD} of the steady detonation is defined by

$$f_{OD} = (D/D_{CJ})^2, \quad (3.1)$$

where D_{CJ} is the Chapman–Jouguet Mach number at which $f_{OD} = 1$, and is given by

$$D_{CJ} = \left[\left(1 + \frac{\gamma^2 - 1}{\gamma} Q \right) + \left[\left(1 + \frac{\gamma^2 - 1}{\gamma} Q \right)^2 - 1 \right]^{1/2} \right]^{1/2}, \quad (3.2)$$

for a given heat release Q . In a frame of reference n attached to the steady detonation shock, such that

$$n = n^l + (\tilde{D}/\tilde{c}_s^*)t, \quad (3.3)$$

where n^l denotes the laboratory-frame horizontal coordinate and the detonation structure lies in the region $n > 0$, the steady pressure, density, velocity and temperature variation through the wave can be calculated from the Rankine–Hugoniot relations as

$$\left. \begin{aligned} p^* &= a + (\gamma^{-1} - a)(1 - bQ(1 - Y^*))^{1/2}, & u^* &= \frac{(1 - \gamma p^*)}{\gamma M_s} + M_s, & v^* &= 0, \\ \rho^* &= M_s/u^*, & T^* &= \gamma p^*/\rho^*, \end{aligned} \right\} \quad (3.4)$$

where

$$M_s = \left[\frac{2 + (\gamma - 1)D^2}{2\gamma D^2 - (\gamma - 1)} \right]^{1/2}, \quad a = \frac{\gamma^{-1}(1 + \gamma D^2)}{2\gamma D^2 + 1 - \gamma}, \quad b = \frac{2(\gamma^2 - 1)D^2}{\gamma(D^2 - 1)^2}. \quad (3.5)$$

It is easily verified that when $D = D_{CJ}$ and the reaction is complete, i.e. when $Y^* = 0$ the flow in the burnt gas is exactly sonic. In order to complete the description of the steady detonation structure, the distribution of the reactant mass fraction must be determined through the integral equation

$$n = -\frac{\beta\theta}{\mathcal{H}} \int_1^{Y^*} \frac{u^*}{Y^*} \exp \left[-\theta \left(1 - \frac{1}{T^*} \right) \right] dY^*. \quad (3.6)$$

3.1. Square-wave structure

In the asymptotic limit of high activation energy where $\theta \gg 1$, the steady detonation assumes the form of a square-wave detonation consisting of an induction zone with weak chemical heat release, terminated by a thin fire zone leading into a uniform chemical equilibrium (or burnt) state. The induction state is determined by expanding the variables ρ , p , u , v , T and Y in the form

$$\mathbf{z}^* = \mathbf{z}_s^* + \frac{1}{\theta} \mathbf{z}_1^*(n) + O\left(\frac{1}{\theta^2}\right), \quad (3.7)$$

where

$$\mathbf{z} = [\rho, u, v, p, T, Y]^T, \quad \mathbf{z}_s^* = [1, M_s, 0, 1/\gamma, 1, 1]^T. \quad (3.8)$$

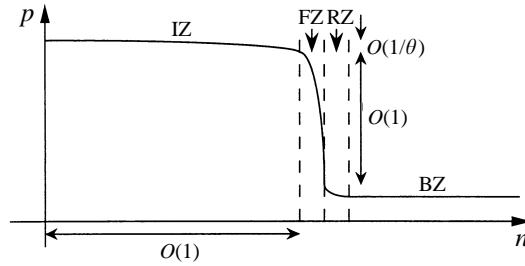


FIGURE 1. A schematic of the structure of the steady limiting square-wave detonation, obtained as $\theta \rightarrow \infty$. The induction zone, fire zone, relaxation zone and equilibrium (or burnt) zone are denoted by IZ, FZ, RZ and BZ respectively.

In the definition of \mathbf{z} we note a dependence between T , p and ρ . However, it is convenient to retain \mathbf{z} in this form for ease of computation later. By substituting the expansion (3.7) into (3.4) and (3.6), it can be verified that the $O(\theta^{-1})$ deviation of the steady induction solution from the post-shock state is determined by the perturbations

$$\left. \begin{aligned} T_1^* &= -\ln(F^* - n), & p_1^* &= -\frac{M_s^2}{\gamma M_s^2 - 1} \ln(F^* - n), & u_1^* &= \frac{M_s}{\gamma M_s^2 - 1} \ln(F^* - n), \\ v_1^* &= 0, & \rho_1^* &= -\frac{1}{\gamma M_s^2 - 1} \ln(F^* - n), & Y_1^* &= \frac{1}{\beta} \frac{M_s^2 - 1}{\gamma M_s^2 - 1} \ln(F^* - n), \end{aligned} \right\} \quad (3.9)$$

where

$$F^* \sim 1 + O(\theta^{-1}) \quad (3.10)$$

is the steady fire location. Thus at $n = 1$, the steady induction-zone perturbation solutions $\mathbf{z}_1^*(n)$ are logarithmically singular, rendering the expansion (3.7) non-uniform. A thin fire zone of rapid reaction, in which the steady variables change by $O(1)$ amounts, and a thin relaxation zone, in which the steady variables deviate by an $O(\theta^{-1})$ amount from their final state, then connect the end of the induction zone to the chemically burnt (or equilibrium) regime. In the standard way, the structure of the fire zone can easily be determined in terms of the $O(1)$ re-scaling variable Σ , where

$$\theta \Sigma = -\ln(F^* - n). \quad (3.11)$$

But since we restrict our present discussions to perturbations with a long wavelength compared to the fire thickness, the fire and relaxation zones can be simply treated as a discontinuous Rankine–Hugoniot deflagration. A schematic of the steady detonation structure in the limit of large activation energy is given in figure 1.

4. Linear stability analysis

The general linear stability problem is formulated by first defining an unsteady shock-attached coordinate system

$$x = n - h(y, t), \quad (4.1)$$

where $h(y, t)$ is the shock displacement in relation to the steady shock location at $n = 0$ and $x = 0$ denotes the shock position in the new coordinate system. The

governing equations (2.11) become in matrix form

$$\mathbf{z}_{,t} + \mathbf{A} \cdot \mathbf{z}_{,x} + \mathbf{B} \cdot \mathbf{z}_{,y} - h_{,t} \mathbf{z}_{,x} - h_{,y} \mathbf{B} \cdot \mathbf{z}_{,x} = \mathbf{c}, \quad (4.2)$$

where the chemical matrix \mathbf{c} is defined as

$$\mathbf{c} = [0, 0, 0, -\beta\rho r, -\gamma\beta r, r]^T, \quad (4.3)$$

and

$$\mathbf{A} = \begin{bmatrix} u & \rho & 0 & 0 & 0 & 0 \\ 0 & u & 0 & 1/\rho & 0 & 0 \\ 0 & 0 & u & 0 & 0 & 0 \\ 0 & \gamma p & 0 & u & 0 & 0 \\ 0 & (\gamma - 1)T & 0 & 0 & u & 0 \\ 0 & 0 & 0 & 0 & 0 & u \end{bmatrix}, \quad \mathbf{B} = \begin{bmatrix} v & 0 & \rho & 0 & 0 & 0 \\ 0 & v & 0 & 0 & 0 & 0 \\ 0 & 0 & v & 1/\rho & 0 & 0 \\ 0 & 0 & \gamma p & v & 0 & 0 \\ 0 & 0 & (\gamma - 1)T & 0 & v & 0 \\ 0 & 0 & 0 & 0 & 0 & v \end{bmatrix}. \quad (4.4)$$

We now seek to determine the stability of the steady detonation wave to small two-dimensional linear perturbations by expanding the variables ρ , p , u , v , T and Y in the normal mode form

$$\mathbf{z} = \mathbf{z}^*(x) + \mathbf{z}'(x)e^{\lambda t}e^{iky}, \quad (4.5)$$

where the prime is used to represent an infinitesimal perturbation quantity. The complex growth rate is given by λ , where $\text{Re}(\lambda)$ defines the real growth rate, $\text{Im}(\lambda)$ the frequency and k the wavenumber of the disturbance. The matrix $\mathbf{z}'(x)$ describes the spatial structure of the perturbation eigenfunctions in the displaced flow. The shock displacement $h(y, t)$ is expanded as

$$h = h'e^{\lambda t}e^{iky}, \quad (4.6)$$

where h' is a constant. By substituting expansions (4.5) and (4.6) into (4.2), the linear perturbation equations are given by

$$\lambda \mathbf{z}' + \mathbf{A}^* \cdot \mathbf{z}'_{,x} + ik \mathbf{B}^* \cdot \mathbf{z}' + (\mathbf{C}_g^* - \mathbf{C}_{ch}^*) \cdot \mathbf{z}' - \lambda h' \mathbf{z}'_{,x} - ik h' \mathbf{B}^* \cdot \mathbf{z}'_{,x} = 0, \quad (4.7)$$

where

$$\mathbf{C}_g^* = \begin{bmatrix} u_{,x} & \rho_{,x} & 0 & 0 & 0 & 0 \\ -p_{,x}/\rho^2 & u_{,x} & 0 & 0 & 0 & 0 \\ 0 & 0 & 0 & 0 & 0 & 0 \\ 0 & p_{,x} & 0 & \gamma u_{,x} & 0 & 0 \\ 0 & T_{,x} & 0 & 0 & (\gamma - 1)u_{,x} & 0 \\ 0 & Y_{,x} & 0 & 0 & 0 & 0 \end{bmatrix}^* \quad (4.8)$$

is a matrix of gasdynamic origin and \mathbf{C}_{ch}^* is a matrix of chemical origin, such that

$$\mathbf{C}_{ch}^* = -\frac{\mathcal{H}}{\beta} r_T \begin{bmatrix} 0 & 0 & 0 & 0 & 0 & 0 \\ 0 & 0 & 0 & 0 & 0 & 0 \\ 0 & 0 & 0 & 0 & 0 & 0 \\ -\beta Y/\theta & 0 & 0 & 0 & -\rho\beta Y/T^2 & -\beta\rho/\theta \\ 0 & 0 & 0 & 0 & -\gamma\beta Y/T^2 & -\gamma\beta/\theta \\ 0 & 0 & 0 & 0 & Y/T^2 & 1/\theta \end{bmatrix}^*, \quad (4.9)$$

where

$$r_T = \exp[\theta(1 - 1/T)]. \quad (4.10)$$

The linearized shock conditions for the perturbation variables are determined from the perturbed Rankine–Hugoniot relations across the detonation shock, which can be solved (Short 1996) in terms of the normal mode perturbation expansions (4.5) and (4.6) as

$$\rho' = \lambda h' \kappa_\rho, \quad u' = \lambda h' \kappa_u, \quad v' = ikh' \kappa_v, \quad p' = \lambda h' \kappa_p, \quad T' = (\gamma - 1)\lambda h' \kappa_T, \quad Y' = 0, \quad (4.11)$$

where

$$\kappa_\rho = \left[\frac{M_s}{M_s^2 - 1} \frac{\mu - 1}{\mu} [2 - (\gamma - 1)(\mu - 1)] \right], \quad (4.12a)$$

$$\kappa_u = \left[\frac{1}{M_s^2 - 1} \frac{\mu - 1}{\mu} [-1 - (1 - (\gamma - 1)(\mu - 1))M_s^2] \right], \quad (4.12b)$$

$$\kappa_v = [M_s(\mu - 1)], \quad (4.12c)$$

$$\kappa_p = \left[\frac{M_s}{M_s^2 - 1} \frac{\mu - 1}{\mu} [2 - (\gamma - 1)(\mu - 1)M_s^2] \right], \quad (4.12d)$$

$$\kappa_T = \left[\frac{M_s}{M_s^2 - 1} \frac{\mu - 1}{\mu} [2 + (\mu - 1)(1 - \gamma M_s^2)] \right]. \quad (4.12e)$$

The parameter μ is given by

$$\mu = \frac{\tilde{\rho}_s^*}{\tilde{\rho}_0^*} = \frac{\tilde{u}_0^*}{\tilde{u}_s^*} = \frac{(\gamma + 1)D^2}{2 + (\gamma - 1)D^2}, \quad (4.13)$$

and is the ratio of the steady post-shock gas density to the unperturbed pre-shock gas density. The conditions (4.11) are applied at $x = 0$. Thus the general linear stability problem is obtained by solving equations (4.7) subject to the shock conditions (4.11), plus an additional condition on the perturbations. For overdriven detonation waves ($f_{OD} > 1$), this condition can, for example, take the form of either a radiation or piston condition on acoustic disturbances in the burnt gas. The former of these conditions, and the radiation condition that is appropriate for Chapman–Jouguet detonation, are discussed in detail in §4.7 and §4.8 below. We now seek a new asymptotic solution to the general stability problem by successively employing the limits of high activation energy and the Newtonian limit in which the specific heats ratio $\gamma \rightarrow 1$.

4.1. *Perturbation equations in the induction zone (IZ)*

An asymptotic solution of the exact linear stability problem (4.7) is now obtained, based first on the limit of large activation energy. In this limit, the steady solution in the induction zone (IZ) is given by expansions (3.7) with solution (3.9), and correspondingly the matrices \mathbf{A}^* , \mathbf{B}^* , \mathbf{C}_g^* , \mathbf{C}_{ch}^* and \mathbf{z}^* have the following asymptotic form in the IZ:

$$\left. \begin{aligned} \mathbf{A}^*(x; \theta) &= \mathbf{A}_0^* + \frac{1}{\theta} \mathbf{A}_1^*(x) + \dots, & \mathbf{B}^*(x; \theta) &= \mathbf{B}_0^* + \frac{1}{\theta} \mathbf{B}_1^*(x) + \dots, \\ \mathbf{C}_g^*(x; \theta) &= \frac{1}{\theta} (\mathbf{C}_g)_1^*(x) + \dots, \\ \mathbf{C}_{ch}^* &= (\mathbf{C}_{ch})_0^*(x) + \frac{1}{\theta} (\mathbf{C}_{ch})_1^*(x) + \dots, & \mathbf{z}^*(x; \theta) &= \mathbf{z}_s^* + \frac{1}{\theta} \mathbf{z}_1^*(x) + \dots, \end{aligned} \right\} \quad (4.14)$$

where

$$\mathbf{A}_0^* = \begin{bmatrix} M_s & 1 & 0 & 0 & 0 & 0 \\ 0 & M_s & 0 & 1 & 0 & 0 \\ 0 & 0 & M_s & 0 & 0 & 0 \\ 0 & 1 & 0 & M_s & 0 & 0 \\ 0 & (\gamma - 1) & 0 & 0 & M_s & 0 \\ 0 & 0 & 0 & 0 & 0 & M_s \end{bmatrix}, \quad \mathbf{B}_0^* = \begin{bmatrix} 0 & 0 & 1 & 0 & 0 & 0 \\ 0 & 0 & 0 & 0 & 0 & 0 \\ 0 & 0 & 0 & 1 & 0 & 0 \\ 0 & 0 & 1 & 0 & 0 & 0 \\ 0 & 0 & (\gamma - 1) & 0 & 0 & 0 \\ 0 & 0 & 0 & 0 & 0 & 0 \end{bmatrix}, \quad (4.15)$$

and

$$(\mathbf{C}_{ch})_0^*(x) = -\frac{\mathcal{K}}{\beta(1-x)} \begin{bmatrix} 0 & 0 & 0 & 0 & 0 & 0 \\ 0 & 0 & 0 & 0 & 0 & 0 \\ 0 & 0 & 0 & 0 & 0 & 0 \\ 0 & 0 & 0 & 0 & -\beta & 0 \\ 0 & 0 & 0 & 0 & -\gamma\beta & 0 \\ 0 & 0 & 0 & 0 & 1 & 0 \end{bmatrix}. \quad (4.16)$$

To the order of accuracy required, we have also explicitly used the leading-order steady fire location $F^* = 1$. Thus the matrices \mathbf{A}^* and \mathbf{B}^* are constant to leading order in the IZ in an expansion in θ^{-1} , while the matrices \mathbf{C}_g^* and \mathbf{z}_x^* are $O(1/\theta)$. The chemical perturbation matrix $(\mathbf{C}_{ch})_0^*(x)$ depends on the spatially varying steady IZ structure, and reflects the singular nature of the IZ structure near the flame front. The expansions (4.14) are now substituted into (4.7) and terms which are explicitly $O(1/\theta)$ are neglected. The perturbation equations (4.7) then reduce to a system involving the standard set of linearized acoustic equations in an inert medium with a chemical forcing term which depends on the temperature perturbation and the steady IZ solution. Specifically, the perturbation equations which are valid in the IZ can be

written as

$$\lambda u' + M_s \frac{du'}{dx} + \frac{dp'}{dx} = 0, \quad (4.17a)$$

$$\lambda v' + M_s \frac{dv'}{dx} + ikp' = 0, \quad (4.17b)$$

$$\lambda p' + M_s \frac{dp'}{dx} + \frac{du'}{dx} + ikv' = \mathcal{K} \frac{T'}{1-x}, \quad (4.17c)$$

$$\lambda T' + M_s \frac{dT'}{dx} + (\gamma - 1) \left(\frac{du'}{dx} + ikv' \right) = \gamma \mathcal{K} \frac{T'}{1-x}, \quad (4.17d)$$

$$\lambda Y' + M_s \frac{dY'}{dx} = -\frac{\mathcal{K}}{\beta} \frac{T'}{1-x}, \quad (4.17e)$$

$$\rho' = \gamma p' - T'. \quad (4.17f)$$

At this stage we make the important observation that the equations (4.17) have been derived based on a large-activation-energy assumption on the steady state. As such the IZ perturbation eigenfunctions equations (4.17) are valid to leading order for any $O(1)$ values of λ or k , large or small. The only requirement for the validity of (4.17) is that the activation energy be sufficiently large, to allow the variation in the gasdynamic spatial structure in the IZ to be neglected. In fact, we note that these equations correspond identically to a linearized two-dimensional version of Clarke's equations (Clarke 1981) in a mean uniform flow. We shall now proceed to provide an asymptotic solution for (4.17) through the use of Newtonian limit asymptotics (Blythe & Crighton 1989).

4.2. Solution of the temperature perturbation in the induction zone in the limit $\gamma \rightarrow 1$

Blythe & Crighton (1989) established that an asymptotic solution of the one-dimensional Clarke's equations (Clarke 1981) could be obtained in the Newtonian limit, in which the ratio of specific heats is assumed to be close to unity. In a recent study of linear stability of the square-wave detonation by Short (1996), this same limit was used to describe the behaviour of the two-dimensional linear stability spectrum through equations (4.17) for disturbances where λ was explicitly order one, $k \sim O(1)$ and $\theta \rightarrow \infty$. In this parameter regime and when $\gamma - 1 \gg \theta^{-1}$, a solution to $O(\gamma - 1)$ for T' was required to determine the spectrum. The excellent agreement with the one-dimensional numerical results of Buckmaster & Neves (1988) has established this limit as an effective tool in detonation stability problems. We shall next proceed to extend the technique developed in Short (1996) to provide a general solution to the linear stability problem for all low-frequency disturbances and arbitrary wavenumbers k , which retains the activation energy as an explicit bifurcation parameter in the problem. To proceed, it is now assumed that the ratio of the isothermal to isentropic sound speeds is close to unity, which for a perfect gas is equivalent to assuming that the ratio of the specific heats is close to unity (Blythe & Crighton 1989), i.e.

$$\gamma - 1 \ll 1. \quad (4.18)$$

In adopting this procedure, we have thus chosen to undertake a sequential limiting process in determining the solution in the IZ, where we let $\theta \rightarrow \infty$ followed by $\gamma \rightarrow 1$, so that the eigenfunction approximation in the IZ to the order with which we are

concerned is valid provided

$$1/\theta \ll \gamma - 1 \ll 1. \quad (4.19)$$

The behaviour of the perturbation eigenfunctions in the induction zone in the Newtonian limit are now found by defining eigenfunction expansions for \mathbf{z}' as

$$\mathbf{z}'(x) = \mathbf{z}'_0(x) + (\gamma - 1)\mathbf{z}'_1(x) + \dots \quad (4.20)$$

By substituting expansions (4.20) into (4.17a-e), the leading-order eigenfunction equations become

$$\lambda u'_0 + M_s \frac{du'_0}{dx} + \frac{dp'_0}{dx} = 0, \quad \lambda v'_0 + M_s \frac{dv'_0}{dx} + ikp'_0 = 0, \quad (4.21a, b)$$

$$\lambda p'_0 + M_s \frac{dp'_0}{dx} + \frac{du'_0}{dx} + ikv'_0 = \frac{M_s}{1-x} T'_0, \quad (4.21c)$$

$$\lambda T'_0 + M_s \frac{dT'_0}{dx} = \frac{M_s}{1-x} T'_0, \quad \lambda Y'_0 + M_s \frac{dY'_0}{dx} = -\frac{M_s}{\beta(1-x)} T'_0, \quad (4.21d, e)$$

where

$$\mathcal{H} = \frac{M_s(M_s^2 - 1)}{\gamma M_s^2 - 1} = M_s + O(\gamma - 1). \quad (4.22)$$

Thus changes in the leading-order temperature and reactant mass fraction perturbations are determined along particle paths only and are independent of changes in the leading-order velocity or pressure perturbations. Under the expansions (4.20), the equations (4.21) are subject to the leading-order shock relations at $x = 0$, obtained from (4.11) as

$$T'_0(0) = 0, \quad Y'_0(0) = 0, \quad p'_0(0) = \lambda h' \kappa_p, \quad u'_0(0) = \lambda h' \kappa_u, \quad v'_0(0) = ikh' \kappa_v, \quad (4.23)$$

where the coefficients κ_p , κ_u and κ_v are treated as known $O(1)$ constants as in Blythe & Crighton (1989). Equation (4.21d) is integrated to give the solution

$$T'_0 = \frac{A}{1-x} e^{-\lambda x/M_s}, \quad (4.24)$$

for constant A . Application of the first of boundary conditions (4.23) shows that to leading order in the expansions (4.20), $A = 0$ and the temperature perturbation within the induction zone must be set everywhere to zero, i.e.

$$T'_0 = 0. \quad (4.25)$$

Also, solving (4.21e) with the second of shock conditions (4.23) gives

$$Y'_0 = 0, \quad (4.26)$$

i.e. the reactant perturbation is also zero everywhere in the induction zone. Thus, to leading order in the Newtonian limit, both the temperature and reactant mass fraction disturbances along particle paths are zero.

With T'_0 determined, (4.21a-c) determine the leading-order pressure and velocity perturbations in the induction zone. Since $T'_0 = 0$ there is no chemical forcing term present in (4.21c), and (4.21a-c) reduce simply to the standard equations of two-dimensional linearized acoustics, with the solution

$$p'_0 = \frac{\lambda^{(1)} - \lambda^{(2)}}{\lambda^{(2)}} M_s A_1 e^{-\lambda^{(2)} x} + \frac{\lambda^{(1)} - \lambda^{(3)}}{\lambda^{(3)}} M_s A_2 e^{-\lambda^{(3)} x}, \quad (4.27a)$$

$$u'_0 = \frac{ikA_3}{\lambda^{(1)}} e^{-\lambda^{(1)}x} + A_1 e^{-\lambda^{(2)}x} + A_2 e^{-\lambda^{(3)}x}, \quad (4.27b)$$

$$v'_0 = A_3 e^{-\lambda^{(1)}x} - \frac{ikA_1}{\lambda^{(2)}} e^{-\lambda^{(2)}x} - \frac{ikA_2}{\lambda^{(3)}} e^{-\lambda^{(3)}x}. \quad (4.27c)$$

The double eigenvalue

$$\lambda^{(1)} = \lambda/M_s, \quad (4.28)$$

corresponds to vorticity and entropy wave propagation in the IZ and

$$\lambda^{(2,3)} = \frac{1}{M_s^2 - 1} \left(M_s \lambda \pm [\lambda^2 - (M_s^2 - 1)k^2]^{1/2} \right) \quad (4.29)$$

corresponds to acoustic wave propagation in the IZ. The root $\lambda^{(3)}$ corresponds to backward-facing characteristic paths which propagate changes at the shock to the fire zone, while the root $\lambda^{(2)}$ corresponds to forward-facing characteristics connecting changes at the flame front to the shock wave. Thus to leading order in the Newtonian limit, the acoustic pressure and velocity disturbances propagate information around the IZ uninfluenced by perturbations in the chemical reaction rate. However, as we shall see below, the role of these acoustic changes is to force $O(\gamma - 1)$ changes in the induction temperature perturbation which, when coupled with $O(\gamma - 1)$ changes in the perturbation shock temperature, lead to a displacement of the fire position relative to its steady value $n = 1$. From the shock conditions (4.23), the coefficients A_1 , A_2 and A_3 are determined as

$$A_1 = \frac{\left(\frac{\lambda^{(1)} - \lambda^{(3)}}{\lambda^{(3)}} \right) \left(M_s \lambda^{(1)} \kappa_u + \frac{k^2}{\lambda^{(1)}} \kappa_v \right) - \left(1 - \frac{k^2}{\lambda^{(1)} \lambda^{(3)}} \right) \lambda^{(1)} \kappa_p h'}{\left(1 - \frac{k^2}{\lambda^{(1)} \lambda^{(2)}} \right) \left(\frac{\lambda^{(1)} - \lambda^{(3)}}{\lambda^{(3)}} \right) - \left(1 - \frac{k^2}{\lambda^{(1)} \lambda^{(3)}} \right) \left(\frac{\lambda^{(1)} - \lambda^{(2)}}{\lambda^{(2)}} \right)}, \quad (4.30a)$$

$$A_2 = \frac{\left(\frac{\lambda^{(1)} - \lambda^{(2)}}{\lambda^{(2)}} \right) \left(M_s \lambda^{(1)} \kappa_u + \frac{k^2}{\lambda^{(1)}} \kappa_v \right) - \left(1 - \frac{k^2}{\lambda^{(1)} \lambda^{(2)}} \right) \lambda^{(1)} \kappa_p h'}{\left(1 - \frac{k^2}{\lambda^{(1)} \lambda^{(3)}} \right) \left(\frac{\lambda^{(1)} - \lambda^{(3)}}{\lambda^{(3)}} \right) - \left(1 - \frac{k^2}{\lambda^{(1)} \lambda^{(2)}} \right) \left(\frac{\lambda^{(1)} - \lambda^{(2)}}{\lambda^{(2)}} \right)}, \quad (4.30b)$$

$$A_3 = ikh' \kappa_v + \frac{ikA_1}{\lambda^{(2)}} + \frac{ikA_2}{\lambda^{(3)}}. \quad (4.30c)$$

At $O(\gamma - 1)$, the equation for $T'_1(x)$ becomes

$$\lambda T'_1 + M_s \frac{dT'_1}{dx} + \frac{du'_0}{dx} + ikv'_0 = \frac{M_s}{1-x} T'_1, \quad (4.31)$$

which is obtained by substituting expansions (4.20) into (4.17d) and collecting terms of $O(\gamma - 1)$. Thus T'_1 is explicitly dependent on the propagation of the leading-order non-forced acoustic disturbances around the IZ. The boundary condition for T'_1 at $x = 0$ is obtained from the shock relations (4.11) as

$$T'_1(0) = \lambda h' \kappa_T, \quad (4.32)$$

where κ_T is again treated as an $O(1)$ constant. Thus T'_1 also depends on changes at the shock front which are propagated along particle paths from the shock into the

IZ. The solution of equation (4.31) is determined as

$$T_1' = \frac{1}{1-x} \left[\frac{\alpha_1}{\lambda^{(2)} - \lambda^{(1)}} e^{\lambda^{(2)}(1-x)} + \frac{\alpha_2}{\lambda^{(3)} - \lambda^{(1)}} e^{\lambda^{(3)}(1-x)} + A_4 e^{\lambda^{(1)}(1-x)} \right] - \alpha_1 e^{\lambda^{(2)}(1-x)} - \alpha_2 e^{\lambda^{(3)}(1-x)}, \quad (4.33)$$

where

$$\left. \begin{aligned} \alpha_1 &= \frac{A_1}{M_s(\lambda^{(2)} - \lambda^{(1)})} \left(\lambda^{(2)} - \frac{k^2}{\lambda^{(2)}} \right) e^{-\lambda^{(2)}}, \\ \alpha_2 &= \frac{A_2}{M_s(\lambda^{(3)} - \lambda^{(1)})} \left(\lambda^{(3)} - \frac{k^2}{\lambda^{(3)}} \right) e^{-\lambda^{(3)}}, \\ A_4 &= \left[M_s \lambda^{(1)} h' \kappa_T - \alpha_1 \left(\frac{1}{\lambda^{(2)} - \lambda^{(1)}} - 1 \right) e^{\lambda^{(2)}} - \alpha_2 \left(\frac{1}{\lambda^{(3)} - \lambda^{(1)}} - 1 \right) e^{\lambda^{(3)}} \right] e^{-\lambda^{(1)}}. \end{aligned} \right\} \quad (4.34)$$

Thus the solution (4.33) emphasizes that T_1' depends equally on the leading-order acoustic wave propagation along the characteristic paths corresponding to $\lambda^{(2)}$ and $\lambda^{(3)}$, and the $O(\gamma - 1)$ changes in the perturbation shock temperature which are propagated along the particle paths corresponding to $\lambda^{(1)}$. It will be shown below that this coupling between acoustic wave propagation and entropy changes results in a perturbation of the fire position relative to its steady position due to the presence of a pole singularity in (4.33) as $x \rightarrow 1$. Before calculating this fire-zone shift, we will now demonstrate how changes in $T'(x)$ at $O(\gamma - 1)$ lead to $O(\gamma - 1)$ changes in the chemical reaction rate in the IZ, which then force $O(\gamma - 1)$ changes in $Y'(x)$, $p'(x)$, $u'(x)$ and $v'(x)$.

4.3. Solution of the reactant mass fraction, pressure and velocity perturbations in the induction zone to $O(\gamma - 1)$.

Having determined the solution of the IZ temperature perturbation $T'(x)$ to $O(\gamma - 1)$, solutions for $Y'(x)$, $p'(x)$, $u'(x)$, $v'(x)$ and $\rho'(x)$ which are correct to $O(\gamma - 1)$ can now be determined directly from equations (4.17) without explicit need to continue with the above expansion procedure. Thus, with

$$T'(x) = (\gamma - 1)T_1'(x), \quad (4.35)$$

the reactant perturbation equation (4.17e) becomes

$$Y_x' + \lambda^{(1)} Y' = -\frac{(M_s^2 - 1)T'(x)}{\beta(\gamma M_s^2 - 1)(1-x)}, \quad (4.36)$$

which is a simple chemically forced linear advection equation. Thus the presence of an $O(\gamma - 1)$ temperature perturbation change leads to an $O(\gamma - 1)$ perturbation in the chemical reaction rate, which in turn forces an $O(\gamma - 1)$ change in the reactant mass fraction. The solution subject to the shock condition $Y'(0) = 0$ is

$$Y'(x) = (\gamma - 1)Y_1'(x), \quad (4.37)$$

where

$$Y_1'(x) = -\frac{M_s^2 - 1}{\beta(\gamma M_s^2 - 1)(1-x)} \left[\frac{\alpha_1 e^{\lambda^{(2)}(1-x)}}{\lambda^{(2)} - \lambda^{(1)}} + \frac{\alpha_2 e^{\lambda^{(3)}(1-x)}}{\lambda^{(3)} - \lambda^{(1)}} + A_4 e^{\lambda^{(1)}(1-x)} \right] + A_5 e^{-\lambda^{(1)}x}, \quad (4.38)$$

and

$$A_5 = \frac{M_s^2 - 1}{\beta(\gamma M_s^2 - 1)} \left[\frac{\alpha_1}{\lambda^{(2)} - \lambda^{(1)}} e^{\lambda^{(2)}} + \frac{\alpha_2}{\lambda^{(3)} - \lambda^{(1)}} e^{\lambda^{(3)}} + A_4 e^{\lambda^{(1)}} \right]. \quad (4.39)$$

By eliminating u' and v' from (4.21a–c), the pressure perturbation can be determined through the equation

$$(M_s^2 - 1) \frac{d^2 p'}{dx^2} + 2M_s \lambda \frac{dp'}{dx} + (\lambda^2 + k^2) p' = \frac{M_s(M_s^2 - 1)}{\gamma M_s^2 - 1} \left[M_s \frac{d}{dx} \left[\frac{T'}{1-x} \right] + \frac{\lambda T'}{1-x} \right], \quad (4.40)$$

which represents the standard second-order linear acoustic pressure disturbance equation with a chemical forcing term. With $p'(x)$ known, the two velocity perturbations are then determined respectively from (4.21a) and (4.21b) as

$$u' = -\frac{e^{-\lambda^{(1)}x}}{M_s} \int \left[\frac{dp'}{dx} \right] e^{\lambda^{(1)}x} dx + \frac{ik}{\lambda^{(1)}} C_3 e^{-\lambda^{(1)}x}, \quad (4.41)$$

and

$$v' = -\frac{ik}{M_s} e^{-\lambda^{(1)}x} \int p' e^{\lambda^{(1)}x} dx + C_3 e^{-\lambda^{(1)}x}, \quad (4.42)$$

where C_3 is a constant which is to be determined from the shock conditions (4.11). Thus the presence of the $O(\gamma - 1)$ temperature perturbation change acts as a source term for $O(\gamma - 1)$ changes in the pressure and velocity perturbations relative to the chemically decoupled propagation of pressure and velocity disturbances around the IZ at leading order in the Newtonian limit expansion. Expanding, the full pressure perturbation equation (4.40) can be written as

$$\begin{aligned} (M_s^2 - 1) \frac{d^2 p'}{dx^2} + 2M_s \lambda \frac{dp'}{dx} + (\lambda^2 + k^2) p' &= (\gamma - 1) \frac{M_s(M_s^2 - 1)}{\gamma M_s^2 - 1} \\ &\times \left\{ \frac{2M_s}{(1-x)^3} \left[\frac{\alpha_1 e^{\lambda^{(2)}(1-x)}}{(\lambda^{(2)} - \lambda^{(1)})} + \frac{\alpha_2 e^{\lambda^{(3)}(1-x)}}{(\lambda^{(3)} - \lambda^{(1)})} + A_4 e^{\lambda^{(1)}(1-x)} \right] \right. \\ &- \frac{2M_s}{(1-x)^2} \left[\alpha_1 e^{\lambda^{(2)}(1-x)} + \alpha_2 e^{\lambda^{(3)}(1-x)} \right] \\ &\left. + \frac{M_s}{1-x} \left[\alpha_1 e^{\lambda^{(2)}(1-x)} (\lambda^{(2)} - \lambda^{(1)}) + \alpha_2 e^{\lambda^{(3)}(1-x)} (\lambda^{(3)} - \lambda^{(1)}) \right] \right\}, \quad (4.43) \end{aligned}$$

which has the general solution

$$p'(x) = M_s \frac{\lambda^{(1)} - \lambda^{(2)}}{\lambda^{(2)}} C_1 e^{-\lambda^{(2)}x} + M_s \frac{\lambda^{(1)} - \lambda^{(3)}}{\lambda^{(3)}} C_2 e^{-\lambda^{(3)}x} + (\gamma - 1) p'_1(x), \quad (4.44)$$

where

$$\begin{aligned} p'_1(x) &= \frac{M_s^2}{\gamma M_s^2 - 1} \left\{ \frac{1}{1-x} \left[\frac{\alpha_1 e^{\lambda^{(2)}(1-x)}}{\lambda^{(2)} - \lambda^{(1)}} + \frac{\alpha_2 e^{\lambda^{(3)}(1-x)}}{\lambda^{(3)} - \lambda^{(1)}} + A_4 e^{\lambda^{(1)}(1-x)} \right] \right. \\ &\left. + \ln(1-x) \left[\alpha_1 \frac{\lambda^{(2)} - \lambda^{(1)}}{\lambda^{(2)} - \lambda^{(3)}} e^{\lambda^{(2)}(1-x)} - \alpha_2 \frac{\lambda^{(3)} - \lambda^{(1)}}{\lambda^{(2)} - \lambda^{(3)}} e^{\lambda^{(3)}(1-x)} \right] \right\} \end{aligned}$$

$$\begin{aligned}
& +e^{\lambda^{(3)}(1-x)}\text{Ei}_1[(\lambda^{(3)} - \lambda^{(2)})(1-x)]\frac{\alpha_1(\lambda^{(3)} - \lambda^{(1)})^2}{(\lambda^{(2)} - \lambda^{(3)})(\lambda^{(2)} - \lambda^{(1)})} \\
& -e^{\lambda^{(2)}(1-x)}\text{Ei}_1[(\lambda^{(2)} - \lambda^{(3)})(1-x)]\frac{\alpha_2(\lambda^{(2)} - \lambda^{(1)})^2}{(\lambda^{(2)} - \lambda^{(3)})(\lambda^{(3)} - \lambda^{(1)})} \\
& -e^{\lambda^{(2)}(1-x)}\text{Ei}_1[(\lambda^{(2)} - \lambda^{(1)})(1-x)]A_4\frac{(\lambda^{(2)} - \lambda^{(1)})^2}{\lambda^{(2)} - \lambda^{(3)}} \\
& +e^{\lambda^{(3)}(1-x)}\text{Ei}_1[(\lambda^{(3)} - \lambda^{(1)})(1-x)]A_4\frac{(\lambda^{(3)} - \lambda^{(1)})^2}{\lambda^{(2)} - \lambda^{(3)}} \Big\}. \tag{4.45}
\end{aligned}$$

$\text{Ei}_1(\zeta)$ is the complex exponential integral

$$\text{Ei}_1(\zeta) = \int_{\zeta}^{\infty} \frac{e^{-t}}{t} dt, \quad |\arg \zeta| < \pi, \tag{4.46}$$

and C_1 and C_2 are constants which are determined below from the shock conditions (4.11). From equation (4.42), the transverse velocity perturbation v' is then given by

$$v'(x) = -\frac{ik}{\lambda^{(2)}}C_1e^{-\lambda^{(2)}x} - \frac{ik}{\lambda^{(3)}}C_2e^{-\lambda^{(3)}x} + C_3e^{-\lambda^{(1)}x} - ik(\gamma - 1)v'_1(x), \tag{4.47}$$

where

$$\begin{aligned}
v'_1(x) = & \frac{M_s}{\gamma M_s^2 - 1} \left\{ -\ln(1-x) \left[\frac{\alpha_1}{\lambda^{(2)} - \lambda^{(3)}} e^{\lambda^{(2)}(1-x)} - \frac{\alpha_2}{\lambda^{(2)} - \lambda^{(3)}} e^{\lambda^{(3)}(1-x)} \right] \right. \\
& -e^{\lambda^{(3)}(1-x)}\text{Ei}_1[(\lambda^{(3)} - \lambda^{(2)})(1-x)]\frac{\alpha_1(\lambda^{(3)} - \lambda^{(1)})}{(\lambda^{(2)} - \lambda^{(3)})(\lambda^{(2)} - \lambda^{(1)})} \\
& +e^{\lambda^{(2)}(1-x)}\text{Ei}_1[(\lambda^{(2)} - \lambda^{(3)})(1-x)]\frac{\alpha_2(\lambda^{(2)} - \lambda^{(1)})}{(\lambda^{(2)} - \lambda^{(3)})(\lambda^{(3)} - \lambda^{(1)})} \\
& +e^{\lambda^{(2)}(1-x)}\text{Ei}_1[(\lambda^{(2)} - \lambda^{(1)})(1-x)]\frac{A_4(\lambda^{(2)} - \lambda^{(1)})}{\lambda^{(2)} - \lambda^{(3)}} \\
& \left. -e^{\lambda^{(3)}(1-x)}\text{Ei}_1[(\lambda^{(3)} - \lambda^{(1)})(1-x)]\frac{A_4(\lambda^{(3)} - \lambda^{(1)})}{\lambda^{(2)} - \lambda^{(3)}} \right\}. \tag{4.48}
\end{aligned}$$

From (4.41), the horizontal velocity perturbation $u'(x)$ is given by

$$u'(x) = C_1e^{-\lambda^{(2)}x} + C_2e^{-\lambda^{(3)}x} + \frac{ik}{\lambda^{(1)}}C_3e^{-\lambda^{(1)}x} + (\gamma - 1)u'_1(x), \tag{4.49}$$

where

$$\begin{aligned}
u'_1(x) = & \frac{M_s}{\gamma M_s^2 - 1} \left\{ -\frac{1}{(1-x)} \left[\frac{\alpha_1 e^{\lambda^{(2)}(1-x)}}{\lambda^{(2)} - \lambda^{(1)}} + \frac{\alpha_2 e^{\lambda^{(3)}(1-x)}}{\lambda^{(3)} - \lambda^{(1)}} + A_4 e^{\lambda^{(1)}(1-x)} \right] \right. \\
& \left. + \ln(1-x) \left[-\frac{\alpha_1 \lambda^{(2)}}{\lambda^{(2)} - \lambda^{(3)}} e^{\lambda^{(2)}(1-x)} + \frac{\alpha_2 \lambda^{(3)}}{\lambda^{(2)} - \lambda^{(3)}} e^{\lambda^{(3)}(1-x)} \right] \right\}
\end{aligned}$$

$$\begin{aligned}
 & -e^{\lambda^{(3)}(1-x)} \text{Ei}_1[(\lambda^{(3)} - \lambda^{(2)})(1-x)] \frac{\alpha_1 \lambda^{(3)}(\lambda^{(3)} - \lambda^{(1)})}{(\lambda^{(2)} - \lambda^{(3)})(\lambda^{(2)} - \lambda^{(1)})} \\
 & + e^{\lambda^{(2)}(1-x)} \text{Ei}_1[(\lambda^{(2)} - \lambda^{(3)})(1-x)] \frac{\alpha_2 \lambda^{(2)}(\lambda^{(2)} - \lambda^{(1)})}{(\lambda^{(2)} - \lambda^{(3)})(\lambda^{(3)} - \lambda^{(1)})} \\
 & + e^{\lambda^{(2)}(1-x)} \text{Ei}_1[(\lambda^{(2)} - \lambda^{(1)})(1-x)] \frac{A_4 \lambda^{(2)}(\lambda^{(2)} - \lambda^{(1)})}{\lambda^{(2)} - \lambda^{(3)}} \\
 & - e^{\lambda^{(3)}(1-x)} \text{Ei}_1[(\lambda^{(3)} - \lambda^{(1)})(1-x)] \frac{A_4 \lambda^{(3)}(\lambda^{(3)} - \lambda^{(1)})}{\lambda^{(2)} - \lambda^{(3)}} \Big\}. \tag{4.50}
 \end{aligned}$$

The density perturbation $\rho'(x)$ is determined to $O(\gamma - 1)$ from (4.21f),

$$\rho' = \gamma p' - T', \tag{4.51}$$

where $p'(x)$ is given by (4.44) and $T'(x)$ is given by (4.35). Finally, the coefficients C_1 , C_2 and C_3 are determined from the shock conditions (4.11) by

$$\begin{aligned}
 C_1 = & \left[\left(\frac{\lambda^{(1)} - \lambda^{(3)}}{\lambda^{(3)}} \right) (M_s \lambda^{(1)} \kappa_u h' - (\gamma - 1) u'_1(0) + \frac{k^2}{\lambda^{(1)}} (\kappa_v h' + (\gamma - 1) v'_1(0))) \right. \\
 & \left. - \frac{1}{M_s} \left(1 - \frac{k^2}{\lambda^{(1)} \lambda^{(3)}} \right) (M_s \lambda^{(1)} \kappa_p h' - (\gamma - 1) p'_1(0)) \right] / \\
 & \left[\left(1 - \frac{k^2}{\lambda^{(1)} \lambda^{(2)}} \right) \left(\frac{\lambda^{(1)} - \lambda^{(3)}}{\lambda^{(3)}} \right) - \left(1 - \frac{k^2}{\lambda^{(1)} \lambda^{(3)}} \right) \left(\frac{\lambda^{(1)} - \lambda^{(2)}}{\lambda^{(2)}} \right) \right], \tag{4.52 a}
 \end{aligned}$$

$$\begin{aligned}
 C_2 = & \left[\left(\frac{\lambda^{(1)} - \lambda^{(2)}}{\lambda^{(2)}} \right) (M_s \lambda^{(1)} \kappa_u h' - (\gamma - 1) u'_1(0) + \frac{k^2}{\lambda^{(1)}} (\kappa_v h' + (\gamma - 1) v'_1(0))) \right. \\
 & \left. - \frac{1}{M_s} \left(1 - \frac{k^2}{\lambda^{(1)} \lambda^{(2)}} \right) (M_s \lambda^{(1)} \kappa_p h' - (\gamma - 1) p'_1(0)) \right] / \\
 & \left[\left(1 - \frac{k^2}{\lambda^{(1)} \lambda^{(3)}} \right) \left(\frac{\lambda^{(1)} - \lambda^{(2)}}{\lambda^{(2)}} \right) - \left(1 - \frac{k^2}{\lambda^{(1)} \lambda^{(2)}} \right) \left(\frac{\lambda^{(1)} - \lambda^{(3)}}{\lambda^{(3)}} \right) \right], \tag{4.52 b}
 \end{aligned}$$

$$C_3 = ik \kappa_v h' + ik(\gamma - 1) v'_1(0) + \frac{ikC_1}{\lambda^{(2)}} + \frac{ikC_2}{\lambda^{(3)}}. \tag{4.52 c}$$

Thus through the formal use of the Newtonian limit where $\gamma \rightarrow 1$, we have succeeded in deriving an asymptotic solution to the eigenfunction structure equations which are valid to $O(\gamma - 1)$ in the IZ of a detonation wave. In order to complete the IZ solution, the response of the fire zone to the presence of the perturbations must now be evaluated. In the following section it will be shown that near the fire, the IZ perturbation solutions possess a simple pole singularity which render the expansions (4.5) non-uniform as $x \rightarrow 1$. It is then necessary to introduce a straining of the steady fire-zone location using the Poincaré–Lighthill–Kuo technique (Nayfeh 1973) in order

to remove the non-uniformity. This analytically calculated straining then corresponds to the shift in the fire-zone location due to the linear perturbations in IZ.

4.4. Fire-zone displacement

Near the fire front, i.e. as $x \rightarrow 1$, the temperature perturbation (4.35) can be shown to behave in the following manner:

$$T' = (\gamma - 1) \left[\frac{\alpha}{1-x} \right] + (\gamma - 1)T'_{1F} + \dots, \quad (4.53)$$

where

$$T'_{1F} = \frac{\alpha_1 \lambda^{(2)}}{\lambda^{(2)} - \lambda^{(1)}} + \frac{\alpha_2 \lambda^{(3)}}{\lambda^{(3)} - \lambda^{(1)}} + A_4 \lambda^{(1)} - \alpha_1 - \alpha_2 = \alpha \lambda^{(1)}, \quad (4.54)$$

and

$$\alpha = \frac{\alpha_1}{\lambda^{(2)} - \lambda^{(1)}} + \frac{\alpha_2}{\lambda^{(3)} - \lambda^{(1)}} + A_4. \quad (4.55)$$

Thus as $x \rightarrow 1$, the temperature perturbation possesses a simple pole singularity. The reactant mass perturbation (4.37) behaviour as $x \rightarrow 1$ is similarly given by

$$Y' = -(\gamma - 1) \frac{M_s^2 - 1}{\beta(\gamma M_s^2 - 1)} \left[\frac{\alpha}{1-x} \right] + (\gamma - 1)Y'_{1F} + \dots, \quad (4.56)$$

where

$$Y'_{1F} = -\frac{M_s^2 - 1}{\beta(\gamma M_s^2 - 1)} \left[\frac{\alpha_1 \lambda^{(2)}}{\lambda^{(2)} - \lambda^{(1)}} + \frac{\alpha_2 \lambda^{(3)}}{\lambda^{(3)} - \lambda^{(1)}} + A_4 \lambda^{(1)} \right] + A_5 e^{-\lambda^{(1)}}, \quad (4.57)$$

which also possesses a simple pole singularity at $x = 1$. Since the exponential integral can be expanded as

$$\text{Ei}_1(\omega(1-x)) = -\gamma^* - \ln(1-x) - \ln \omega + O(1-x), \quad (4.58)$$

as $x \rightarrow 1$, where γ^* is the Euler constant

$$\gamma^* = \lim_{n \rightarrow \infty} \left(\sum_{i=1}^n 1/i - \ln(n) \right) = 0.5772156649, \quad (4.59)$$

the behaviour of the pressure perturbation (4.44) as $x \rightarrow 1$ is given by

$$p' = p'_{0F} + (\gamma - 1) \frac{M_s^2}{\gamma M_s^2 - 1} \left[\frac{\alpha}{1-x} + p'_{0 \ln} \ln(1-x) \right] + (\gamma - 1)p'_{1F} + \dots, \quad (4.60)$$

where

$$p'_{0 \ln} = \alpha(\lambda^{(2)} + \lambda^{(3)} - 2\lambda^{(1)}) = \frac{2\alpha\lambda^{(1)}}{M_s^2 - 1}, \quad (4.61)$$

and

$$p'_{0F} = M_s \frac{\lambda^{(1)} - \lambda^{(2)}}{\lambda^{(2)}} A_1 e^{-\lambda^{(2)}} + M_s \frac{(\lambda^{(1)} - \lambda^{(3)})}{\lambda^{(3)}} A_2 e^{-\lambda^{(3)}}, \quad (4.62 a)$$

$$p'_{1F} = M_s \frac{\lambda^{(1)} - \lambda^{(2)}}{\lambda^{(2)}} B_1 e^{-\lambda^{(2)}} + M_s \frac{(\lambda^{(1)} - \lambda^{(3)})}{\lambda^{(3)}} B_2 e^{-\lambda^{(3)}} \\ + \frac{M_s^2}{\gamma M_s^2 - 1} \left\{ \left[\frac{\alpha_1 \lambda^{(2)}}{\lambda^{(2)} - \lambda^{(1)}} + \frac{\alpha_2 \lambda^{(3)}}{\lambda^{(3)} - \lambda^{(1)}} + A_4 \lambda^{(1)} \right] \right\}$$

$$\begin{aligned}
& - [\gamma^* + \ln(\lambda^{(3)} - \lambda^{(2)})] \alpha_1 \frac{(\lambda^{(3)} - \lambda^{(1)})^2}{(\lambda^{(2)} - \lambda^{(3)})(\lambda^{(2)} - \lambda^{(1)})} \\
& + [\gamma^* + \ln(\lambda^{(2)} - \lambda^{(3)})] \alpha_2 \frac{(\lambda^{(2)} - \lambda^{(1)})^2}{(\lambda^{(2)} - \lambda^{(3)})(\lambda^{(3)} - \lambda^{(1)})} \\
& + [\gamma^* + \ln(\lambda^{(2)} - \lambda^{(1)})] A_4 \frac{(\lambda^{(2)} - \lambda^{(1)})^2}{\lambda^{(2)} - \lambda^{(3)}} \\
& - [\gamma^* + \ln(\lambda^{(3)} - \lambda^{(1)})] A_4 \frac{(\lambda^{(3)} - \lambda^{(1)})^2}{\lambda^{(2)} - \lambda^{(3)}} \Big\}. \tag{4.62 b}
\end{aligned}$$

The constants B_1 and B_2 are determined from an expansion of C_1 and C_2 (4.52) in terms of $\gamma - 1$ as

$$C_1 = A_1 + (\gamma - 1)B_1, \quad C_2 = A_2 + (\gamma - 1)B_2, \tag{4.63}$$

so that

$$B_1 = \frac{\left(\frac{\lambda^{(1)} - \lambda^{(3)}}{\lambda^{(3)}}\right) \left(-u'_1(0) + \frac{k^2}{\lambda^{(1)}} v'_1(0)\right) + \frac{1}{M_s} \left(1 - \frac{k^2}{\lambda^{(1)}\lambda^{(3)}}\right) p'_1(0)}{\left(1 - \frac{k^2}{\lambda^{(1)}\lambda^{(2)}}\right) \left(\frac{\lambda^{(1)} - \lambda^{(3)}}{\lambda^{(3)}}\right) - \left(1 - \frac{k^2}{\lambda^{(1)}\lambda^{(3)}}\right) \left(\frac{\lambda^{(1)} - \lambda^{(2)}}{\lambda^{(2)}}\right)}, \tag{4.64 a}$$

$$B_2 = \frac{\left(\frac{\lambda^{(1)} - \lambda^{(2)}}{\lambda^{(2)}}\right) \left(-u'_1(0) + \frac{k^2}{\lambda^{(1)}} v'_1(0)\right) + \frac{1}{M_s} \left(1 - \frac{k^2}{\lambda^{(1)}\lambda^{(2)}}\right) p'_1(0)}{\left(1 - \frac{k^2}{\lambda^{(1)}\lambda^{(3)}}\right) \left(\frac{\lambda^{(1)} - \lambda^{(2)}}{\lambda^{(2)}}\right) - \left(1 - \frac{k^2}{\lambda^{(1)}\lambda^{(2)}}\right) \left(\frac{\lambda^{(1)} - \lambda^{(3)}}{\lambda^{(3)}}\right)}. \tag{4.64 b}$$

Thus in addition to the simple pole which appears in (4.60) as $x \rightarrow 1$, a weaker logarithmic singularity is also present in the $O(\gamma - 1)$ correction term. The behaviour of the horizontal velocity perturbation $u'(x)$ as $x \rightarrow 1$ can be determined from (4.49) as

$$u'(x) = u'_{0F} - (\gamma - 1) \frac{M_s}{\gamma M_s^2 - 1} \left[\frac{\alpha}{1 - x} + u'_{0 \ln} \ln(1 - x) \right] + (\gamma - 1) u'_{1F} + \dots, \tag{4.65}$$

where

$$u'_{0 \ln} = \alpha(\lambda^{(3)} + \lambda^{(2)} - \lambda^{(1)}) = \frac{(M_s^2 + 1)\alpha\lambda^{(1)}}{M_s^2 - 1}, \tag{4.66}$$

and

$$u'_{0F} = A_1 e^{-\lambda^{(2)}} + A_2 e^{-\lambda^{(3)}} + \frac{ik}{\lambda^{(1)}} A_3 e^{-\lambda^{(1)}}, \tag{4.67 a}$$

$$\begin{aligned}
u'_{1F} &= B_1 e^{-\lambda^{(2)}} + B_2 e^{-\lambda^{(3)}} + \frac{ik}{\lambda^{(1)}} B_3 e^{-\lambda^{(1)}} \\
&+ \frac{M_s}{\gamma M_s^2 - 1} \left\{ - \left[\frac{\alpha_1 \lambda^{(2)}}{\lambda^{(2)} - \lambda^{(1)}} + \frac{\alpha_2 \lambda^{(3)}}{\lambda^{(3)} - \lambda^{(1)}} + A_4 \lambda^{(1)} \right] \right\}
\end{aligned}$$

$$\begin{aligned}
&+(\gamma^* + \ln(\lambda^{(3)} - \lambda^{(2)})) \frac{\alpha_1 \lambda^{(3)} (\lambda^{(3)} - \lambda^{(1)})}{(\lambda^{(2)} - \lambda^{(3)}) (\lambda^{(2)} - \lambda^{(1)})} \\
&- (\gamma^* + \ln(\lambda^{(2)} - \lambda^{(3)})) \frac{\alpha_2 \lambda^{(2)} (\lambda^{(2)} - \lambda^{(1)})}{(\lambda^{(2)} - \lambda^{(3)}) (\lambda^{(3)} - \lambda^{(1)})} \\
&- (\gamma^* + \ln(\lambda^{(2)} - \lambda^{(1)})) \frac{A_4 \lambda^{(2)} (\lambda^{(2)} - \lambda^{(1)})}{\lambda^{(2)} - \lambda^{(3)}} \\
&+(\gamma^* + \ln(\lambda^{(3)} - \lambda^{(1)})) \frac{A_4 \lambda^{(3)} (\lambda^{(3)} - \lambda^{(1)})}{\lambda^{(2)} - \lambda^{(3)}} \Big\}. \tag{4.67 b}
\end{aligned}$$

The constant B_3 is again determined from an expansion of C_3 (4.52) in terms of $\gamma - 1$ as

$$C_3 = A_3 + (\gamma - 1)B_3, \tag{4.68}$$

so that

$$B_3 = ikv'_1(0) + \frac{ikB_1}{\lambda^{(2)}} + \frac{ikB_2}{\lambda^{(3)}}. \tag{4.69}$$

The behaviour of the transverse velocity component $v'(x)$ as $x \rightarrow 1$ can be obtained from (4.47) and is given by

$$v'(x) = v'_{0F} - ik(\gamma - 1) \frac{M_s}{\gamma M_s^2 - 1} v'_{0 \ln} \ln(1 - x) + (\gamma - 1)v'_{1F} + \dots, \tag{4.70}$$

where

$$v'_{0 \ln} = -\alpha, \tag{4.71}$$

and

$$v'_{0F} = -\frac{ik}{\lambda^{(2)}} A_1 e^{-\lambda^{(2)}} - \frac{ik}{\lambda^{(3)}} A_2 e^{-\lambda^{(3)}} + A_3 e^{-\lambda^{(1)}} \tag{4.72 a}$$

$$\begin{aligned}
v'_{1F} = &-\frac{ik}{\lambda^{(2)}} B_1 e^{-\lambda^{(2)}} - \frac{ik}{\lambda^{(3)}} B_2 e^{-\lambda^{(3)}} + B_3 e^{-\lambda^{(1)}} \\
&- ik \frac{M_s}{\gamma M_s^2 - 1} \Big\{ (\gamma^* + \ln(\lambda^{(3)} - \lambda^{(2)})) \frac{\alpha_1 (\lambda^{(3)} - \lambda^{(1)})}{(\lambda^{(2)} - \lambda^{(3)}) (\lambda^{(2)} - \lambda^{(1)})} \\
&- (\gamma^* + \ln(\lambda^{(2)} - \lambda^{(3)})) \frac{\alpha_2 (\lambda^{(2)} - \lambda^{(1)})}{(\lambda^{(2)} - \lambda^{(3)}) (\lambda^{(3)} - \lambda^{(1)})} \\
&- (\gamma^* + \ln(\lambda^{(2)} - \lambda^{(1)})) \frac{A_4 (\lambda^{(2)} - \lambda^{(1)})}{\lambda^{(2)} - \lambda^{(3)}} \\
&+(\gamma^* + \ln(\lambda^{(3)} - \lambda^{(1)})) \frac{A_4 (\lambda^{(3)} - \lambda^{(1)})}{\lambda^{(2)} - \lambda^{(3)}} \Big\}. \tag{4.72 b}
\end{aligned}$$

We note that only the weaker logarithmic singularity is present in the expansion (4.70) for $v'(x)$ as $x \rightarrow 1$ and the pole singularity does not appear. Finally, the behaviour of

the IZ density perturbation $\rho'(x)$ as $x \rightarrow 1$ is given by

$$\rho' = \rho'_{0F} + (\gamma - 1) \frac{1}{\gamma M_s^2 - 1} \left[\frac{\alpha}{1-x} + \rho'_{0\ln} \ln(1-x) \right] + (\gamma - 1) \rho'_{1F} + \dots, \quad (4.73)$$

where

$$\rho'_{0F} = \gamma p'_{0F}, \quad \rho'_{0\ln} = \gamma M_s^2 p'_{0\ln}, \quad \rho'_{1F} = \gamma p'_{1F} - T'_{1F}. \quad (4.74)$$

In order to understand the role of the pole singularities which appear in expansions (4.53), (4.56), (4.60), (4.65) and (4.73), these perturbation singularities can be combined with the steady solution (3.9) with $F^* = 1$ and the expansions (4.5) written in the following form:

$$T \sim 1 - \frac{1}{\theta} \ln(1-x) + (\gamma - 1) \frac{\alpha}{1-x} e^{iky} e^{\lambda t} + \dots, \quad (4.75 a)$$

$$Y \sim 1 + \frac{M_s^2 - 1}{\beta(\gamma M_s^2 - 1)} \left[\frac{1}{\theta} \ln(1-x) - (\gamma - 1) \frac{\alpha}{1-x} e^{iky} e^{\lambda t} \right] + \dots, \quad (4.75 b)$$

$$p \sim \frac{1}{\gamma} - \frac{M_s^2}{\gamma M_s^2 - 1} \left[\frac{1}{\theta} \ln(1-x) - (\gamma - 1) \frac{\alpha}{1-x} e^{iky} e^{\lambda t} \right] + \dots, \quad (4.75 c)$$

$$u \sim M_s + \frac{M_s}{\gamma M_s^2 - 1} \left[\frac{1}{\theta} \ln(1-x) - (\gamma - 1) \frac{\alpha}{1-x} e^{iky} e^{\lambda t} \right] + \dots, \quad (4.75 d)$$

$$\rho \sim 1 - \frac{1}{\gamma M_s^2 - 1} \left[\frac{1}{\theta} \ln(1-x) - (\gamma - 1) \frac{\alpha}{1-x} \right] e^{iky} e^{\lambda t} + \dots, \quad (4.75 e)$$

as $x \rightarrow 1$. Thus the presence of the pole singularities as $x \rightarrow 1$ in the perturbation quantities introduces a non-uniformity in the expansions (4.5) near the fire front. Essentially, the non-uniformity develops due to the failure to account for perturbations in the fire-front position that are generated by the small unsteady perturbations in the IZ. This classical type of non-uniformity can be removed by straining the location of the fire front by an application of the method of strained coordinates, or Poincaré–Lighthill–Kuo technique (Nayfeh 1973). After doing so, equations (4.75) can then be shown to take the regular form

$$\left. \begin{aligned} T &\sim 1 - \frac{1}{\theta} \ln(F(y,t) - x) + \dots, & Y &\sim 1 + \frac{M_s^2 - 1}{\theta \beta (\gamma M_s^2 - 1)} \ln(F(y,t) - x) + \dots, \\ p &\sim \frac{1}{\gamma} - \frac{M_s^2}{\theta (\gamma M_s^2 - 1)} \ln(F(y,t) - x) + \dots, & u &\sim M_s + \frac{M_s}{\theta (\gamma M_s^2 - 1)} \ln(F(y,t) - x) + \dots, \\ \rho &\sim 1 - \frac{1}{\theta (\gamma M_s^2 - 1)} \ln(F(y,t) - x) + \dots, \end{aligned} \right\} \quad (4.76)$$

where

$$x = F(y,t) = 1 + \theta [(\gamma - 1)F'_0 + (\gamma - 1)^2 F'_1] e^{iky} e^{\lambda t}, \quad (4.77)$$

and

$$F'_0 = -\alpha \quad (4.78)$$

gives the leading-order perturbation in the position of the fire about $x = F^* \sim 1$,

corresponding to the presence of the unsteady perturbations in the IZ. The quantity F'_1 is the first-order correction which would be determined by taking the IZ expansions to an additional order in $(\gamma - 1)$. Thus in order to remove the non-uniformity in expansions (4.75), the position of the fire has to be shifted by an amount $O((\gamma - 1)\theta\alpha)$. We also note that relative to the steady-shock coordinate system, n , the perturbation in fire position about the steady fire-zone location $n = F^* \sim 1$ is given by

$$n = 1 + \widehat{F}'_0 e^{iky} e^{\lambda t}, \quad (4.79)$$

where

$$\widehat{F}'_0 = h' - \theta(\gamma - 1)\alpha. \quad (4.80)$$

4.5. Behaviour as $x \rightarrow F(y, t)$

After removing the pole singularity in equations (4.53), (4.56), (4.60), (4.65) and (4.73), we note an additional non-uniformity in the expansions (4.60), (4.65), (4.70) and (4.73) due to the presence of the $\ln(F(y, t) - x)$ terms, which occurs when

$$\sigma = -(\gamma - 1) \ln(F(y, t) - x) \sim O(1). \quad (4.81)$$

Since $(\gamma - 1) \gg \theta^{-1}$, this non-uniformity occurs in a thin layer upstream of the main fire zone. The behaviour of the IZ perturbations in this layer is determined by seeking an expansion of \mathbf{z} in the form

$$\mathbf{z} = \mathbf{z}_s^* + \frac{1}{\theta} \mathbf{z}'_1 (1 - e^{-\sigma/(\gamma-1)}) + \mathbf{z}' e^{iky} e^{\lambda t} + \dots \quad (4.82)$$

Substituting the expansions (4.82) into (2.11), the perturbations eigenfunctions \mathbf{z}' can be shown to satisfy the equations

$$\mathbf{A}_0^* \cdot \mathbf{z}'_\sigma e^{iky} e^{\lambda t} - \frac{F_t}{\theta} \mathbf{z}'_{1\sigma} - \frac{F_y}{\theta} \mathbf{B}_0 \cdot \mathbf{z}'_{1\sigma} = \frac{(\mathbf{C}_{ch}^*)_0 \cdot \mathbf{z}'}{\gamma - 1} e^{iky} e^{\lambda t} e^{-\sigma/(\gamma-1)}, \quad (4.83)$$

or individually,

$$(M_s u'_\sigma + p'_\sigma) e^{iky} e^{\lambda t} + \frac{M_s}{\theta(\gamma M_s^2 - 1)} \frac{F_t}{\gamma - 1} = 0, \quad (4.84a)$$

$$v'_\sigma e^{iky} e^{\lambda t} - \frac{M_s}{\theta(\gamma M_s^2 - 1)} \frac{F_y}{\gamma - 1} = 0, \quad (4.84b)$$

$$(u'_\sigma + M_s p'_\sigma) e^{iky} e^{\lambda t} - \frac{M_s^2}{\theta(\gamma M_s^2 - 1)} \frac{F_t}{\gamma - 1} = \frac{M_s(M_s^2 - 1)}{\gamma M_s^2 - 1} \frac{T'}{\gamma - 1} e^{iky} e^{\lambda t}, \quad (4.84c)$$

$$((\gamma - 1)u'_\sigma + M_s T'_\sigma) e^{iky} e^{\lambda t} - \frac{F_t}{\theta(\gamma - 1)} = \frac{M_s T'}{\gamma - 1} e^{iky} e^{\lambda t}, \quad (4.84d)$$

$$M_s Y'_\sigma e^{iky} e^{\lambda t} + \frac{(M_s^2 - 1)}{\theta\beta(\gamma M_s^2 - 1)} \frac{F_t}{\gamma - 1} = -\frac{M_s(M_s^2 - 1)}{(\gamma M_s^2 - 1)} \frac{T'}{\beta(\gamma - 1)} e^{iky} e^{\lambda t}. \quad (4.84e)$$

The equations (4.84) are solved by introducing the Newtonian limit expansions

$$\mathbf{z}' = \mathbf{z}'_0 + (\gamma - 1)\mathbf{z}'_1, \quad F = 1 + \theta(-(\gamma - 1)\alpha + (\gamma - 1)^2 F'_1) e^{iky} e^{\lambda t}, \quad (4.85)$$

and solutions for \mathbf{z}'_0 and \mathbf{z}'_1 found by substituting expansions (4.85) into (4.84) and solving successively at $O(1)$ and $O(\gamma - 1)$. Matching with the main induction-layer

solutions (4.53), (4.56), (4.60), (4.65), (4.70) and (4.73) in the limit $\sigma \rightarrow 0$ leads to the following perturbation solutions, which are valid to $O(\gamma - 1)$ in the thin layer upstream of the fire:

$$T' = (\gamma - 1)T'_{1F}, \quad (4.86a)$$

$$Y' = (\gamma - 1) \left(\frac{M_s^2 - 1}{\beta(\gamma M_s^2 - 1)} Y'_{1\ln} \sigma + Y'_{1F} \right), \quad (4.86b)$$

$$p' = \left(-\frac{M_s^2}{\gamma M_s^2 - 1} p'_{0\ln} \sigma + p'_{0F} \right) + (\gamma - 1) \left(-\frac{M_s^2}{\gamma M_s^2 - 1} p'_{1\ln} \sigma + p'_{1F} \right), \quad (4.86c)$$

$$u' = \left(\frac{M_s}{\gamma M_s^2 - 1} u'_{0\ln} \sigma + u'_{0F} \right) + (\gamma - 1) \left(\frac{M_s}{\gamma M_s^2 - 1} u'_{1\ln} \sigma + u'_{1F} \right), \quad (4.86d)$$

$$v' = \left(\frac{ikM_s}{\gamma M_s^2 - 1} v'_{0\ln} \sigma + v'_{0F} \right) + (\gamma - 1) \left(\frac{ikM_s}{\gamma M_s^2 - 1} v'_{1\ln} \sigma + v'_{1F} \right), \quad (4.86e)$$

$$\rho' = \left(-\frac{1}{\gamma M_s^2 - 1} \rho'_{0\ln} \sigma + \rho'_{0F} \right) + (\gamma - 1) \left(-\frac{1}{\gamma M_s^2 - 1} \rho'_{1\ln} \sigma + \rho'_{1F} \right), \quad (4.86f)$$

where

$$\left. \begin{aligned} Y'_{1\ln} &= -\frac{\alpha\lambda(M_s^2 + 1)}{M_s(\gamma M_s^2 - 1)(M_s^2 - 1)}, & p'_{1\ln} &= -\frac{2\lambda^{(1)}F'_1}{M_s^2 - 1} - \frac{\alpha\lambda^{(1)}(M_s^2 + 1)}{(\gamma M_s^2 - 1)(M_s^2 - 1)}, \\ u'_{1\ln} &= -\frac{(M_s^2 + 1)\lambda^{(1)}F'_1}{M_s^2 - 1} - \frac{\alpha\lambda^{(1)}(M_s^2 + 1)}{(\gamma M_s^2 - 1)(M_s^2 - 1)}, & v'_{1\ln} &= F'_1, & \rho'_{1\ln} &= \gamma M_s^2 p'_{1\ln}. \end{aligned} \right\} \quad (4.87)$$

A referee has pointed out that as $x \rightarrow F(y, t)$, the perturbed linear system can be shown to have the general limiting behaviour

$$\mathbf{z}' = \mathbf{G}(\gamma - 1)\sigma + \mathbf{H}(\gamma - 1) + \text{exp. small in } \sigma/(\gamma - 1), \quad (4.88)$$

in which for general γ , the constant matrix \mathbf{G} can be found by direct substitution, while the constant matrix \mathbf{H} must be obtained by matching with a numerical solution of the IZ equations. For the present analysis, both \mathbf{G} and \mathbf{H} are determined analytically to $O(\gamma - 1)$. Combined with equations (4.76), the IZ solution can finally be written as

$$T \sim 1 + \frac{1}{\theta(\gamma - 1)}\sigma + (\gamma - 1)T'_{1F}e^{iky}e^{\lambda t} + \dots, \quad (4.89a)$$

$$Y \sim 1 - \frac{M_s^2 - 1}{\theta(\gamma - 1)\beta(\gamma M_s^2 - 1)}\sigma + (\gamma - 1) \left[\frac{M_s^2 - 1}{\beta(\gamma M_s^2 - 1)} Y'_{1\ln} \sigma + Y'_{1F} \right] e^{iky}e^{\lambda t} + \dots, \quad (4.89b)$$

$$p \sim \frac{1}{\gamma} + \frac{M_s^2}{\theta(\gamma - 1)\gamma M_s^2 - 1}\sigma + \left[\left(-\frac{M_s^2}{\gamma M_s^2 - 1} p'_{0\ln} \sigma + p'_{0F} \right) + (\gamma - 1) \left(-\frac{M_s^2}{\gamma M_s^2 - 1} p'_{1\ln} \sigma + p'_{1F} \right) \right] e^{iky}e^{\lambda t} + \dots, \quad (4.89c)$$

$$u \sim M_s - \frac{M_s}{\theta(\gamma-1)(\gamma M_s^2-1)}\sigma + \left[\left(\frac{M_s}{\gamma M_s^2-1} u'_{0\ln}\sigma + u'_{0F} \right) + (\gamma-1) \left(\frac{M_s}{\gamma M_s^2-1} u'_{1\ln}\sigma + u'_{1F} \right) \right] e^{iky} e^{\lambda t} + \dots, \quad (4.89d)$$

$$v \sim \left[\left(\frac{ikM_s}{\gamma M_s^2-1} v'_{0\ln}\sigma + v'_{0F} \right) + (\gamma-1) \left(\frac{ikM_s}{\gamma M_s^2-1} v'_{1\ln}\sigma + v'_{1F} \right) \right] e^{iky} e^{\lambda t} + \dots, \quad (4.89e)$$

$$\rho \sim 1 + \frac{1}{\theta(\gamma-1)(\gamma M_s^2-1)}\sigma + \left[\left(-\frac{1}{\gamma M_s^2-1} \rho'_{0\ln}\sigma + \rho'_{0F} \right) + (\gamma-1) \left(-\frac{1}{\gamma M_s^2-1} \rho'_{1\ln}\sigma + \rho'_{1F} \right) \right] e^{iky} e^{\lambda t} + \dots. \quad (4.89f)$$

Provided $(\gamma-1)^2 = O(\theta^{-1})$ or $(\gamma-1)^2 \ll \theta^{-1}$, the next breakdown in expansions (4.89) occurs when $\sigma = O(\theta(\gamma-1))$, or when $-\ln(F(y,t)-x) = O(\theta)$, i.e. where the IZ terminates and the solution enters the main reaction layer. We are now in a position to complete the stability analysis, first by calculating the behaviour of the linearized perturbations in the burnt zone, and subsequently matching this behaviour to the expansions (4.89) across the fire zone.

4.6. Burnt-zone perturbations

With reference to figure 1, in the limit of large activation energy an exponentially small fire region (FZ) and exponentially small relaxation region (RZ) connect the induction zone to the burnt zone (BZ) in which reaction has terminated, i.e. where

$$Y = \text{exp. small terms} \quad \text{as} \quad \theta \rightarrow \infty. \quad (4.90)$$

The linear perturbations to the steady state in the BZ are determined by an expansion in the normal mode form (Buckmaster and Ludford 1987),

$$\mathbf{z} = \mathbf{z}_b^* + \mathbf{z}'_b(x) e^{\lambda t} e^{iky}, \quad (4.91)$$

where the subscript b is used to denote BZ quantities. Substituting expansions (4.91) into (2.11) with $Y = 0$, the pressure and velocity perturbation eigenfunctions in the BZ are determined by the standard two-dimensional linear acoustic equations

$$\lambda u'_b + M_b v_b \frac{du'_b}{dx} + \frac{1}{\mu_b} \frac{dp'_b}{dx} = 0, \quad (4.92a)$$

$$\lambda v'_b + M_b v_b \frac{dv'_b}{dx} + \frac{ik}{\mu_b} p'_b = 0, \quad (4.92b)$$

$$\lambda p'_b + M_b v_b \frac{dp'_b}{dx} + v_b^2 \mu_b \left(\frac{du'_b}{dx} + ikv'_b \right) = 0, \quad (4.92c)$$

where M_b , μ_b and v_b are given by

$$M_b = \frac{\tilde{u}_b^*}{\tilde{c}_b^*}, \quad \mu_b = \frac{\tilde{\rho}_b^*}{\tilde{\rho}_s^*}, \quad v_b = \frac{\tilde{c}_b^*}{\tilde{c}_s^*}, \quad (4.93)$$

and represent the Mach number of the steady flow in the BZ, the ratio of the unperturbed material density in the BZ to that at the detonation shock and the ratio of the unperturbed adiabatic sound speed in the BZ to that at the detonation shock. The two velocity perturbations u'_b and v'_b can be eliminated from (4.92) to give the second-order linear equation for p'_b ,

$$(M_b^2 - 1)v_b \frac{d^2 p'_b}{dx^2} + 2\lambda M_b \frac{dp'_b}{dx} + v_b \left(k^2 + \frac{\lambda^2}{v_b^2} \right) p'_b = 0. \quad (4.94)$$

For $M_b < 1$, i.e. when the detonation is overdriven and the flow in the BZ is subsonic, the characteristic roots of equation (4.94) are given by

$$\lambda_b^{(2,3)} = -\frac{1}{v_b(M_b^2 - 1)} [M_b \lambda \pm [\lambda^2 + k^2 v_b^2 (1 - M_b^2)]^{1/2}], \quad (4.95)$$

and correspond to the surfaces of acoustic wave propagation in the BZ. The root $\lambda_b^{(2)}$ represents upstream propagation from infinity to the rear of the fire, while the root $\lambda_b^{(3)}$ represents downstream propagation from the fire. On the other hand, for $M_b = 1$, i.e. when the steady detonation is travelling at the Chapman–Jouguet velocity and the flow in the BZ is exactly sonic, the linear equation (4.94) is degenerate and one of the characteristic roots in (4.94) is eliminated. The remaining characteristic root is given by

$$\lambda_b^{(4)} = -\frac{v_b}{2\lambda} \left(k^2 + \frac{\lambda^2}{v_b^2} \right), \quad (4.96)$$

which corresponds to downstream propagation from the fire. The fact that the upstream root is eliminated is due to the particular nature of the sonic flow. The presence of the sonic point at the end of the fire zone dictates that the BZ and detonation wave are acoustically decoupled, and perturbations originating downstream of the fire are unable to penetrate into the detonation structure. This has significant implications for the determination of a compatibility condition in the linear stability analysis, as will be discussed below. For $M_b < 1$, the general solution to (4.94) is given by

$$p'_b = A_{1b} e^{\lambda_b^{(2)} x} + A_{2b} e^{\lambda_b^{(3)} x}, \quad (4.97 a)$$

$$u'_b = -\frac{ikA_{3b}}{\lambda_b^{(1)}} e^{\lambda_b^{(1)} x} - \frac{\lambda_b^{(2)} A_{1b} e^{\lambda_b^{(2)} x}}{M_b \mu_b v_b (\lambda_b^{(2)} - \lambda_b^{(1)})} - \frac{\lambda_b^{(3)} A_{2b} e^{\lambda_b^{(3)} x}}{M_b \mu_b v_b (\lambda_b^{(3)} - \lambda_b^{(1)})}, \quad (4.97 b)$$

$$v'_b = A_{3b} e^{\lambda_b^{(1)} x} - \frac{ikA_{1b} e^{\lambda_b^{(2)} x}}{M_b \mu_b v_b (\lambda_b^{(2)} - \lambda_b^{(1)})} - \frac{ikA_{2b} e^{\lambda_b^{(3)} x}}{M_b \mu_b v_b (\lambda_b^{(3)} - \lambda_b^{(1)})}, \quad (4.97 c)$$

for constants A_{1b} , A_{2b} , A_{3b} , where

$$\lambda_b^{(1)} = -\frac{\lambda}{M_b v_b} \quad (4.98)$$

corresponds to vorticity and entropy wave propagation in the BZ. When $M_b = 1$, the general solution to (4.94) is given by

$$p'_b = A_{4b} e^{\lambda_b^{(4)} x}, \quad (4.99 a)$$

$$u'_b = -\frac{ikA_{5b}}{\lambda_b^{(5)}} e^{\lambda_b^{(5)}x} - \frac{\lambda_b^{(4)} A_{4b} e^{\lambda_b^{(4)}x}}{\mu_b v_b (\lambda_b^{(4)} - \lambda_b^{(5)})}, \quad (4.99b)$$

$$v'_b = A_{5b} e^{\lambda_b^{(5)}x} - \frac{ikA_{4b} e^{\lambda_b^{(4)}x}}{\mu_b v_b (\lambda_b^{(4)} - \lambda_b^{(5)})}, \quad (4.99c)$$

for constants A_{4b} , A_{5b} , where

$$\lambda_b^{(5)} = -\frac{\lambda}{v_b}, \quad (4.100)$$

also corresponds to vorticity and entropy wave propagation in the BZ, but when $M_b = 1$.

4.7. Radiation condition for overdriven detonation waves

For overdriven detonation waves, i.e. when $M_b < 1$, a condition on the perturbations in the BZ is required in order to determine a linear dispersion relation. For the present analysis we employ a standard acoustic radiation condition in the BZ in which the root $\lambda_b^{(2)}$, which represents upstream propagation from infinity, is eliminated (Buckmaster & Ludford 1987). Therefore we set

$$A_{1b} = 0, \quad (4.101)$$

and equations (4.97) lead to the compatibility relation,

$$\lambda u'_b - ikM_b v_b v'_b - \frac{p'_b}{\mu_b v_b} [\lambda^2 + k^2 v_b^2 (1 - M_b^2)]^{1/2} = 0, \quad (4.102)$$

for perturbations in the BZ. For one-dimensional disturbances, i.e. when $k = 0$, the compatibility relation (4.102) reduces to

$$u'_b = \frac{p'_b}{v_b \mu_b}. \quad (4.103)$$

It should be noted that for overdriven detonation waves, the relation (4.102) is not unique in determining a condition on the behaviour of perturbations in the burnt gas. One could, for example, easily impose a piston-type condition where the velocity perturbation far downstream of the detonation is zero. Conditions of this type will be considered in a future article, but for the present, the condition (4.102) is used in order to compare the results obtained from the asymptotic analysis with available numerical results. However, we note that Lee & Stewart (1990) established that employing a piston condition, rather than a radiation condition, leads only to minor quantitative changes in the eigenvalue λ .

4.8. Radiation condition for Chapman–Jouguet detonation waves

When $M_b = 1$, the sonic condition eliminates the upstream-propagating acoustic waves automatically. The three equations (4.99) then comprise the two unknown constants A_{4b} and A_{5b} . Thus for a regular solution, the equations (4.99) must necessarily satisfy the compatibility relation

$$\lambda u'_b - ik v_b v'_b - \frac{\lambda p'_b}{\mu_b v_b} = 0. \quad (4.104)$$

We note that this is simply the limiting form of the acoustic radiation condition (4.102) for overdriven detonation waves when $M_b \rightarrow 1$. However, unlike the situation

for the overdriven detonation, the Chapman–Jouguet detonation must necessarily satisfy the condition (4.104) in the burnt zone, and there is no arbitrariness in the specification of a compatibility condition. As such, it will be demonstrated below that we must then impose a further compatibility condition on the jump relations across the fire zone for the Chapman–Jouguet detonation in order to complete the specification of the linear stability problem.

4.9. Rankine–Hugoniot deflagration relations across the discontinuous fire zone

Having determined the behaviour of the linear perturbation quantities in the burnt and induction zones of the detonation wave, we are now required to match these quantities across the fire and relaxation zones. In the limit of high activation energy these zones are exponentially small, and providing the wavelength of the disturbance is sufficiently long, the fire and relaxation zones can be treated as a standard Rankine–Hugoniot discontinuity with heat addition (Buckmaster & Ludford 1987). For very high-frequency disturbances, the structure of the flame zone must be accounted for in the linear stability analysis. This analysis is not treated here. In this work, we limit our attention to wavelengths that are much longer than the fire-zone thickness. Substituting the BZ expansions (4.91) and the IZ expansions (4.89) at the front of the fire zone into the Rankine–Hugoniot deflagration relations across the perturbed fire zone, whose location is given by (4.79), leads to the equations

$$\mu_b(u'_b - \lambda\widehat{F}'_0) + M_b v_b \rho'_b = (u'_F - \lambda\widehat{F}'_0) + M_s \rho'_F, \quad (4.105 a)$$

$$p'_b + \mu_b v_b M_b (2u'_b - \lambda\widehat{F}'_0) + v_b^2 M_b^2 \rho'_b = p'_F + M_s (2u'_F - \lambda\widehat{F}'_0) + M_s^2 \rho'_F, \quad (4.105 b)$$

$$\left(\frac{\gamma}{\mu_b} p'_b - \frac{v_b^2}{\mu_b} \rho'_b \right) + (\gamma - 1) M_b v_b (u'_b - \lambda\widehat{F}'_0) = \beta Y'_F + (\gamma p'_F - \rho'_F) + (\gamma - 1) M_s (u'_F - \lambda\widehat{F}'_0), \quad (4.105 c)$$

$$ik v_b M_b \widehat{F}'_0 + v'_b = ik M_s \widehat{F}'_0 + v'_F, \quad (4.105 d)$$

which relate the induction quantities \mathbf{z}'_F evaluated at the fire to the burnt perturbations \mathbf{z}'_b . Also,

$$\left. \begin{aligned} T'_F &= (\gamma - 1) T'_{1F}, & p'_F &= p'_{0F} + (\gamma - 1) p'_{1F}, & \rho'_F &= \rho'_{0F} + (\gamma - 1) \rho'_{1F}, \\ Y'_F &= (\gamma - 1) Y'_{1F}, & u'_F &= u'_{0F} + (\gamma - 1) u'_{1F}, & v'_F &= v'_{0F} + (\gamma - 1) v'_{1F}. \end{aligned} \right\} \quad (4.106)$$

We note that to the order of the analysis concerned in the IZ, the terms involving σ in the relations (4.89) cancel out when substituted into the Rankine–Hugoniot relations. In particular, the perturbation terms in σ simply account for the modification in the quasi-steady fire structure from the steady location $n = F^* \sim 1$ to its new location $n = 1 + \widehat{F}'_0 \exp(iky) \exp(\lambda t)$, and thus would be expected to cancel out in the Rankine–Hugoniot relations (cf. Short 1996, appendix A). Equations (4.105 a–c) can be put into matrix form as

$$\mathbf{A}_b \cdot \mathbf{e}'_b = \begin{bmatrix} M_s \\ M_s^2 \\ -1 \end{bmatrix} \rho'_F + \begin{bmatrix} 1 \\ 2M_s \\ (\gamma - 1)M_s \end{bmatrix} u'_F + \begin{bmatrix} 0 \\ 1 \\ \gamma \end{bmatrix} p'_F + \begin{bmatrix} 0 \\ 0 \\ \beta \end{bmatrix} Y'_F$$

$$+ \begin{bmatrix} \mu_b - 1 \\ 0 \\ (\gamma - 1)(M_b v_b - M_s) \end{bmatrix} \lambda \widehat{F}'_0, \quad (4.107)$$

where

$$\mathbf{e}'_b = [\rho'_b, u'_b, p'_b]^T, \quad \mathbf{A}_b = \begin{bmatrix} M_b v_b & \mu_b & 0 \\ v_b^2 M_b^2 & 2\mu_b v_b M_b & 1 \\ -v_b^2/\mu_b & (\gamma - 1)M_b v_b & \gamma/\mu_b \end{bmatrix}. \quad (4.108)$$

For $M_b < 1$, the matrix \mathbf{A}_b has the inverse

$$\mathbf{A}_b^{-1} = \frac{1}{(M_b^2 - 1)} \begin{bmatrix} \frac{M_b}{v_b}(\gamma + 1) & -\frac{\gamma}{v_b^2} & \frac{\mu_b}{v_b^2} \\ -\frac{\gamma M_b^2 + 1}{\mu_b} & \frac{\gamma M_b}{\mu_b v_b} & -\frac{M_b}{v_b} \\ v_b M_b((\gamma - 1)M_b^2 + 2) & -((\gamma - 1)M_b^2 + 1) & M_b^2 \mu_b \end{bmatrix}, \quad (4.109)$$

so that explicit relations for u'_b and p'_b can be written down in terms of \widehat{F}'_0 , ρ'_F , u'_F , p'_F and Y'_F as

$$\begin{aligned} u'_b &= \lambda \widehat{F}'_0 \left[\frac{1}{M_b^2 - 1} \frac{\mu_b - 1}{\mu_b} \left[-1 - (1 - (\gamma - 1)(\mu_b - 1))M_b^2 \right] \right. \\ &\quad \left. - \rho'_F \left[\frac{v_b M_b}{M_b^2 - 1} \left[-\frac{1}{v_b^2} + 1 + ((1 - \mu_b) + (\gamma - 1)(1 - \mu_b))M_b^2 \right] \right] \right. \\ &\quad \left. - u'_F \left[\frac{1}{\mu_b(M_b^2 - 1)} \left[1 + (1 - 2\mu_b + (\gamma - 1)(\mu_b - 1)^2)M_b^2 \right] \right] \right. \\ &\quad \left. - p'_F \left[\frac{\gamma}{\mu_b v_b} \frac{M_b}{(M_b^2 - 1)} (\mu_b - 1) \right] - Y'_F \beta \frac{M_b}{v_b(M_b^2 - 1)} \right], \quad (4.110) \end{aligned}$$

and

$$\begin{aligned} p'_b &= \lambda \widehat{F}'_0 \left[\frac{\mu_b v_b M_b}{M_b^2 - 1} \frac{\mu_b - 1}{\mu_b} \left[2 - (\gamma - 1)(\mu_b - 1)M_b^2 \right] \right. \\ &\quad \left. + \rho'_F \left[\frac{v_b^2 \mu_b M_b^2}{M_b^2 - 1} \left[-\frac{1}{v_b^2} + 2 - \mu_b - (\gamma - 1)(\mu_b - 1)M_b^2 \right] \right] \right. \\ &\quad \left. + u'_F \left[\frac{v_b \mu_b M_b}{M_b^2 - 1} \frac{1 - \mu_b}{\mu_b} \left[2 - (\gamma - 1)(\mu_b - 1)M_b^2 \right] \right] \right. \\ &\quad \left. + p'_F \left[\frac{1}{M_b^2 - 1} \left[-1 + (\mu_b + (\gamma - 1)(\mu_b - 1))M_b^2 \right] \right] + Y'_F \beta \mu_b \frac{M_b^2}{M_b^2 - 1}, \quad (4.111) \end{aligned}$$

From (4.105d), the transverse velocity perturbation v'_b is given by

$$v'_b = ikv_b M_b \widehat{F}'_0 (\mu_b - 1) + v'_F. \quad (4.112)$$

Thus for $M_b < 1$, the dispersion relation is obtained by substituting the relations (4.110)–(4.112) into the radiation condition (4.102) and solving for λ using a Newton–Raphson iteration method.

For $M_b = 1$, the matrix \mathbf{A}_b^{-1} is singular. In §4.8 above, it was established that for $M_b = 1$ the burnt perturbations must necessarily satisfy the radiation condition (4.104), and thus (4.105 a–c) are no longer independent. For $M_b < 1$ these equations are independent and can be inverted. However, for $M_b = 1$ the condition (4.104) must be satisfied and this accounts for the singularity in \mathbf{A}_b^{-1} . The compatibility condition required on the perturbations at the fire front to eliminate this singularity is then obtained by using (4.105a) to eliminate u'_b from (4.105 b) and (4.105 c) and subtracting the resulting equations. This leads to the dispersion relation

$$\begin{aligned} \gamma \left(\frac{1}{\mu_b} - 1 \right) p'_F + \frac{v_b}{\mu_b} (\mu_b - 1) [\gamma + 1 - (\gamma - 1)\mu_b] u'_F + (v_b^2 (\gamma \mu_b - (\gamma + 1)) + 1) \rho'_F \\ - \beta Y'_F + \frac{\mu_b - 1}{\mu_b} v_b [-(\gamma + 1) + (\gamma - 1)\mu_b] \lambda \widehat{F}'_0 = 0. \end{aligned} \quad (4.113)$$

Thus for Chapman–Jouguet detonation waves the relations \mathbf{z}'_F are now substituted into the compatibility relation (4.113), which is solved directly to determine the eigenvalue λ using Newton–Raphson iteration. Using conditions (4.113) and (4.104), the relations (4.105) can now be solved for u'_b , ρ'_b and p'_b to give

$$\begin{aligned} u'_b = \frac{1}{2\mu_b v_b} \left[p'_F + u'_F v_b (2\mu_b - 1) + \mu_b v_b^2 (\mu_b - 1) \rho'_F - v_b \lambda \widehat{F}'_0 (\mu_b - 1) \right. \\ \left. + \frac{ik}{\lambda} \mu_b v_b^2 v'_F + \frac{ik}{\lambda} \mu_b v_b^3 (\mu_b - 1) ik \widehat{F}'_0 \right], \end{aligned} \quad (4.114 a)$$

$$\begin{aligned} \rho'_b = \frac{1}{2v_b^2} \left[-p'_F + u'_F v_b (3 - 2\mu_b) + \mu_b v_b^2 \rho'_F (3 - \mu_b) + 3v_b (\mu_b - 1) \lambda \widehat{F}'_0 \right. \\ \left. - \frac{ik}{\lambda} \mu_b v_b^2 v'_F - \frac{ik}{\lambda} \mu_b v_b^3 (\mu_b - 1) ik \widehat{F}'_0 \right], \end{aligned} \quad (4.114 b)$$

$$p'_b = \mu_b v_b u'_b - \frac{ik}{\lambda} \mu_b v_b^2 \left(ik v_b (\mu_b - 1) \widehat{F}'_0 + v'_F \right). \quad (4.114 c)$$

Finally, we note that a unified dispersion relation for both overdriven and Chapman–Jouguet detonation waves can be obtained in the form of (4.113) as a compatibility condition on the four equations; this comprises the radiation condition (4.102) and the three jump relations (4.105 a–c) in the three unknowns p'_b , u'_b and ρ'_b , since v'_b is determined from (4.112) for both overdriven and detonation waves. This leads to the following dispersion relation which is valid for $M_b \leq 1$:

$$R_1 p'_F + R_2 \rho'_F + R_3 Y'_F + R_4 u'_F + R_5 v'_F + \lambda R_6 \widehat{F}'_0 + ik R_7 \widehat{F}'_0 = 0, \quad (4.115)$$

where

$$R_1 = \gamma [\lambda^2 + k^2 v_b^2 (1 - M_b^2)]^{1/2} (1 - M_b^2) + \gamma \delta \left(\frac{1}{\mu_b} - 1 \right), \quad (4.116a)$$

$$R_2 = - \left[\gamma \lambda v_b^2 M_b + (1 + (\gamma - 1) v_b^2 M_b^2) [\lambda^2 + k^2 v_b^2 (1 - M_b^2)]^{1/2} \right] (1 - M_b^2) \\ + \delta [v_b^2 M_b^2 (\gamma \mu_b - (\gamma + 1)) + 1], \quad (4.116b)$$

$$R_3 = \beta [\lambda^2 + k^2 v_b^2 (1 - M_b^2)]^{1/2} (1 - M_b^2) - \delta \beta, \quad (4.116c)$$

$$R_4 = \frac{v_b}{\mu_b} \left[-\gamma \lambda + (\gamma - 1) M_b (\mu_b^2 - 1) [\lambda^2 + k^2 v_b^2 (1 - M_b^2)]^{1/2} \right] (1 - M_b^2) \\ + \delta \frac{\mu_b - 1}{\mu_b} v_b M_b [\gamma + 1 - (\gamma - 1) \mu_b], \quad (4.116d)$$

$$R_5 = \gamma i k M_b v_b^2 (1 - M_b^2), \quad (4.116e)$$

$$R_6 = \left[-\gamma v_b \lambda - (\gamma - 1) (\mu_b + 1) M_b v_b [\lambda^2 + k^2 v_b^2 (1 - M_b^2)]^{1/2} \right] \\ \times \frac{\mu_b - 1}{\mu_b} (1 - M_b^2) + \delta [-(\gamma + 1) + (\gamma - 1) \mu_b] \frac{\mu_b - 1}{\mu_b} M_b v_b, \quad (4.116f)$$

$$R_7 = \gamma i k v_b^3 M_b^2 (\mu_b - 1) (1 - M_b^2) \quad (4.116g)$$

and

$$\delta = \gamma \lambda M_b + (1 + (\gamma - 1) M_b^2) [\lambda^2 + k^2 v_b^2 (1 - M_b^2)]^{1/2}. \quad (4.117)$$

It is easy to verify that when $M_b = 1$, the general dispersion relation (4.115) reduces to (4.113).

5. The mechanism of linear detonation instability

With the analytical theory developed in §4, we can now describe the physical mechanisms behind the generation of hydrodynamic detonation instabilities. The mechanism implied by this analysis both reinforces and clarifies the thermal-acoustic generation of the instability put forward in Aouseif & Toong (1982, 1986). To leading order in the Newtonian limit, §4.2 shows that the effects of an unsteady perturbation of the detonation shock are propagated around the induction zone by acoustic pressure disturbances independently of any perturbation in the chemical reaction rate. The leading-order acoustic perturbation behaviour at the fire zone is determined by a matching problem across the fire into the equilibrium (or burnt) zone, where an acoustic radiation condition is employed. When corrections of $O(\gamma - 1)$ are ignored, (4.80) shows that there is no perturbation in the fire-zone location relative to the shock perturbation, i.e. the fire-zone location (4.79) is given by $n = 1 + h' \exp[iky + \lambda t]$. In this case, it can be shown by numerical evaluation of the dispersion relation (4.115) that the detonation is stable to all disturbances, i.e. $\text{Re}(\lambda) < 0$ for all detonation

parameters. Stability prevails since the acoustic energy associated with the disturbance is ultimately lost from the system. Firstly, right-travelling acoustic disturbances which strike the fire and are transmitted into the burnt zone are propagated away from the detonation due to the radiation condition. Secondly, left-travelling waves, which are reflected from the fire and return to the shock, are diminished in amplitude after reflection from the shock. Thus, without any sustaining mechanism for the acoustic perturbations, the detonation returns to a steady state.

The multi-dimensional instability of the detonation wave must therefore be associated with sustained fire-zone oscillations in both the normal and transverse planes, which act as an oscillating energy source (Abouseif & Toong 1982, 1986). From (4.79) and (4.80), these oscillations can only occur when $\gamma > 1$. In the general case, the amplitude and period of the fire-zone oscillation are influenced by two hydrodynamic processes. Firstly, as the leading-order reaction-rate-independent, pressure wave propagation occurs in the IZ along the paths corresponding to $\lambda^{(2)}$ and $\lambda^{(3)}$, $O(\gamma - 1)$ acoustic temperature fluctuations are generated. Due to the three-wave acoustic-entropy system present in the linearized form of Clarke's equations (4.17) (Clarke 1981), and the presence of the chemical kinetic forcing term at $O(\gamma - 1)$, these pressure fluctuations are the source of $O(\gamma - 1)$ temperature changes which occur along the entropy paths corresponding to $\lambda^{(1)}$, and lead to fluctuations in the fire-zone location. Also, $O(\gamma - 1)$ changes in temperature are generated along the entropy paths $\lambda^{(1)}$ which depend directly on the $O(\gamma - 1)$ temperature perturbation at the shock. These two processes combine in the IZ to determine the overall fire-zone perturbation (4.79). Abouseif & Toong (1982, 1986) state that the acoustic temperature changes could reasonably be neglected in favour of the entropy changes generated at the shock. For the present analysis, these two components are of the same order.

The compatibility condition (4.115), obtained by matching the IZ perturbations to the burnt perturbations across the fire front, shows clearly that the fire-zone displacement then influences the leading-order acoustic field, thus establishing a feedback cycle between acoustic wave propagation, entropy changes and the fire-zone displacement. For the range of detonation parameters within which these factors can sustain an undamped oscillation of the fire-zone location, instability will result. As above, the damping mechanism is associated with the loss of acoustic energy through the fire into the burnt zone, and through reflection of acoustic waves at the shock. The exact criterion for instability must be obtained from the dispersion relation (4.115), where instability results from the range of detonation parameters which cause $\text{Re}(\lambda) > 0$. Thus we conclude that the mechanism of detonation instability is generated by an intricate acoustic-thermal interaction. Instability mechanisms which neglect part or all of this interaction in the general case are too simplistic for $O(1)$ detonation Mach numbers. What is not clear, though, from the identification of the instability mechanism above is an understanding of how a linear theory might predict the observed detonation cell spacing in nonlinear two-dimensional problems. Additional observations on this issue are made below in §6.

For very low-frequency instabilities, the mechanisms are more simple than that described above. Specifically, when the frequency is $O(\theta^{-1})$, Buckmaster & Ludford (1987) have shown that the leading-order fire-zone perturbation results directly from the $O(\gamma - 1)$ temperature perturbation at the shock, which is propagated along entropy paths towards the fire. Acoustic effects are relegated to higher order. In this case the detonation is always unstable, since there is no restoring mechanism for the fire-zone perturbation available in the Buckmaster & Ludford (1987) analysis. Depending on the sign of the temperature perturbation, the fire will either move monotonically

toward (for a positive temperature perturbation) or recede from (for a negative temperature perturbation) the shock. Yao & Stewart (1996) have shown that either the detonation can be stabilized, or an oscillatory mechanism of instability can be established, by accounting for the higher-order acoustic effects absent from the Buckmaster & Ludford (1987) analysis. For a certain range of parameters, inclusion of these acoustic effects in the IZ analysis leads to an oscillatory instability of the fire-zone location, akin to that observed in a forced linear oscillator system. Alternatively, the inclusion of the acoustic effects can be shown to lead to neutrally stable or unconditionally stable detonation waves, as determined by the dispersion relation derived in Yao & Stewart (1996).

Having determined the role played by the fire-zone displacement in establishing the instability of the detonation wave, it becomes apparent why increases in θ , increases in γ , decreases in Q and decreases in f_{OD} can lead to instability. When $\gamma > 1$, it can be seen from (4.79) and (4.80) that the fire-zone displacements in the normal and transverse directions are proportional to $\theta(\gamma - 1)$. Sustained perturbations in the fire-zone location are required for instability. The stronger the fire-zone displacement, the stronger the damping mechanism required to attain stability. Thus increases in θ or γ lead directly to increases in $\partial F/\partial t$ and $\partial F/\partial y$, which by virtue of the relation (4.115) can overcome the damping mechanisms and lead to instability. Also, due to the post-shock temperature scaling of the dimensional activation energy, decreases in Q at fixed f_{OD} and decreases in f_{OD} at fixed Q lead to increases in θ and thus to increases in $\partial F/\partial t$ and $\partial F/\partial y$. We also note that for sufficiently large θ , the dispersion relation (4.115) reduces to that previously derived by Short (1996) for the stability of the classical square-wave detonation when $(\gamma - 1) \gg \theta^{-1}$, which is unconditionally unstable.

6. Dispersion relation and linear stability spectrum

We now present a comparison of the behaviour of the low-frequency unstable mode predicted by the asymptotic dispersion relation (4.115) with exact numerical solutions of the linear stability spectrum (Short 1997). The growth rates and frequencies obtained from (4.115) are rescaled in terms of the time scaling used in Short (1997), i.e. the post-shock steady adiabatic sound speed multiplied by the half-reaction length. Similarly, wavenumbers are presented in terms of the half-reaction length. Conversion factors between the scalings used for deriving the analytical results above and those used to generate the numerical results can be found in Lee & Stewart (1990). The comparisons below are shown for realistic regimes of the detonation parameters, including those for Chapman-Jouguet detonations as well as overdriven detonations.

Figure 2 shows the migration of the growth rate $\text{Re}(\lambda)$ and frequency $\text{Im}(\lambda)$ of the lowest-frequency mode calculated from the analytical dispersion relation (4.115) as the activation energy E varies for $Q = 50$, $f_{OD} = 1.2$ and $\gamma = 1.2$. Also shown is the result of a direct numerical solution of the linear disturbance equations (4.7) for $Q = 50$, $f_{OD} = 1.2$ and $\gamma = 1.2$. The asymptotic solution mimics precisely the behaviour of the numerical solution and additionally offers a fair quantitative approximation to the numerical results. In particular, the asymptotic theory predicts that the low-frequency root is stable for $E < 17.1$, i.e. for sufficiently low activation energies. This compares to a value of $E = 30.6$ obtained from the numerical solution. As E increases, the asymptotic solution predicts that the growth rate increases, until at $E = 42.8$ the oscillatory mode bifurcates into two non-oscillatory modes. The numerically calculated value of the bifurcation point is $E = 52.8$. Subsequently, the

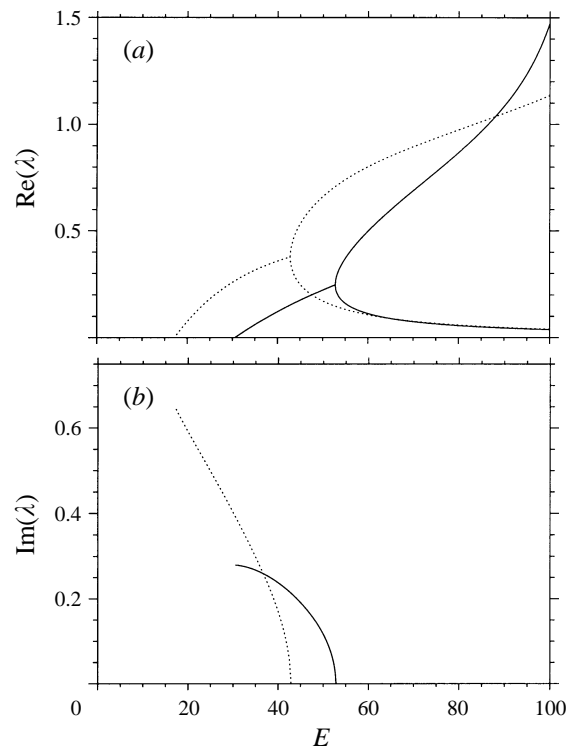


FIGURE 2. The migration of (a) the growth rate $\text{Re}(\lambda)$ and (b) the frequency $\text{Im}(\lambda)$ with activation energy E of the one-dimensional low-frequency linear disturbance, as calculated numerically in Short (1997) (solid lines) and asymptotically (dotted lines) from (4.115) with $Q = 50$, $\gamma = 1.2$ and $f_{OD} = 1.2$.

growth rate of one mode increases, while the growth rate of the other non-oscillatory mode decreases. Short (1997) has established that the lower branch corresponds to that identified asymptotically in Buckmaster & Ludford (1987). For $E > 60$, the asymptotic and numerical solutions for the lower branch coincide. For the upper branch, the asymptotic solution remains a good approximation to the numerical solution, even though the growth rates are becoming large.

Figure 3 shows a comparison of the migration of the growth rate $\text{Re}(\lambda)$ and frequency $\text{Im}(\lambda)$ with activation energy E of the one-dimensional low-frequency disturbance, which is predicted from the asymptotic theory (4.115), with a direct numerical solution for the exact low-frequency spectrum with $Q = 50$, $\gamma = 1.2$ and $f_{OD} = 1$, i.e. for a Chapman–Jouguet detonation wave. In this case, the dispersion relation results from the compatibility condition on the fire-zone jump conditions §4.8. Again, the agreement in the behaviour of the two solutions is favourable. Values above $E = 60$ were difficult to obtain numerically due to the nature of the sonic condition in Chapman–Jouguet waves. A comparable behaviour for the linear stability spectrum is observed in this Chapman–Jouguet case as that seen in the previous overdriven case (figure 2). The dispersion relation (4.115) predicts that the detonation is stable for a sufficiently low activation energy, in this case for $E < 12.4$, compared to a numerical value of $E < 25.3$. Growth rates increase with increasing E and bifurcate into two non-oscillatory modes at $E = 23.9$ (asymptotic solution) and

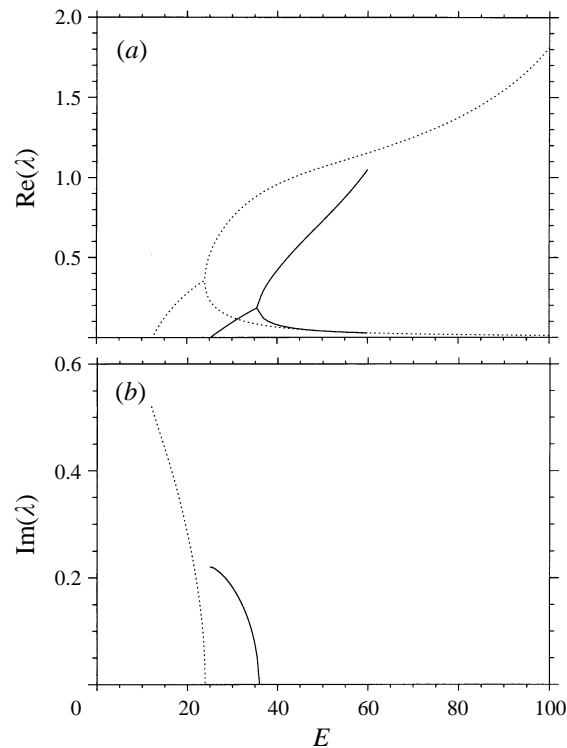


FIGURE 3. The migration of (a) the growth rate $\text{Re}(\lambda)$ and (b) the frequency $\text{Im}(\lambda)$ with activation energy E of the one-dimensional low-frequency linear disturbance, as calculated numerically in Short (1997) (solid lines) and asymptotically (dotted lines) from (4.115) with $Q = 50$, $\gamma = 1.2$ and $f_{OD} = 1$.

$E = 35.5$ (numerical solution). For $E > 42$, the lower branch of the non-oscillatory mode coincides with the numerical solution.

Figure 4 shows a comparison of the much studied case of the migration of the growth rate $\text{Re}(\lambda)$ and frequency $\text{Im}(\lambda)$ with detonation overdrive f_{OD} , for the one-dimensional low-frequency disturbance predicted from the dispersion relation (4.115), with an exact numerical solution for $Q = 50$, $\gamma = 1.2$ and $E = 50$. Again, the asymptotic solution mimics precisely the behaviour of the exact numerical solution and predicts stability for $f_{OD} > 2.34$, compared to a numerical value of $f_{OD} > 1.73$. Predictions of the stability boundary with the detonation overdrive f_{OD} as the bifurcation parameter have been the source of most of the direct numerical simulations of detonation instability (Fickett & Wood 1966; Bourlioux *et al.* 1991; Quirk 1994). The asymptotic solution predicts that at $f_{OD} = 2.34$ a Hopf bifurcation occurs in the low-frequency root, rendering the detonation unstable. For further decreases in overdrive, the growth rate of this oscillatory mode is predicted to increase. At $f_{OD} = 1.29$ this mode bifurcates into two non-oscillatory modes. This compares to a numerical value of $f_{OD} = 1.16$. At $f_{OD} = 1$, there are two non-oscillatory modes with growth rates determined from (4.115) as $\text{Re}(\lambda) = 0.040$ and $\text{Re}(\lambda) = 1.065$.

Figure 5 is a prediction of the one-dimensional Chapman–Jouguet neutral stability curve in the activation energy (E)–heat release (Q) plane for the low-frequency mode with $\gamma = 1.2$ and $f_{OD} = 1$, as obtained from the dispersion relation (4.115). The neutral stability curve marks the boundary between one-dimensional stability and

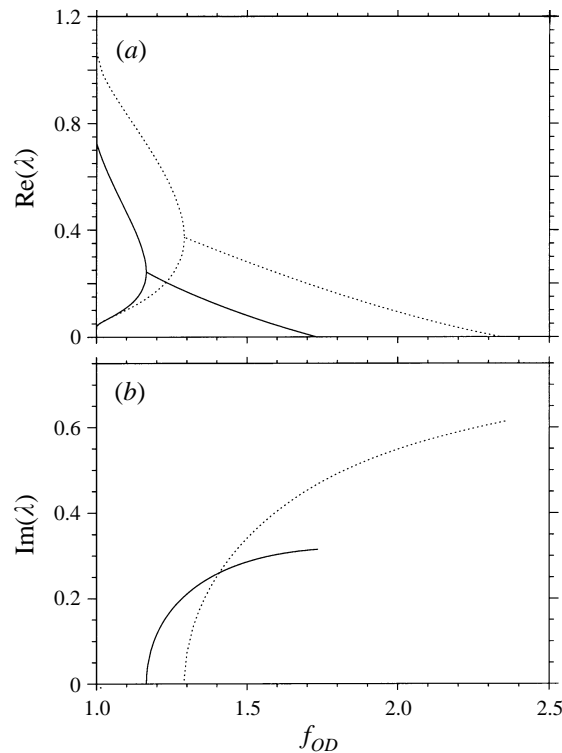


FIGURE 4. The migration of (a) the growth rate $\text{Re}(\lambda)$ and (b) the frequency $\text{Im}(\lambda)$ with detonation overdrive f_{OD} of the one-dimensional low-frequency linear disturbance, as calculated numerically in Short (1997) (solid lines) and asymptotically (dotted lines) from (4.115) with $Q = 50$, $E = 50$ and $\gamma = 1.2$.

instability of the detonation wave and shows that increases in E at fixed Q can render the detonation unstable.

Figures 6–11 show a series of results on the linear stability behaviour corresponding to two-dimensional low-frequency disturbances. Figure 6 shows a comparison of the migration of the growth rate $\text{Re}(\lambda)$ and frequency $\text{Im}(\lambda)$ with wavenumber k for the two-dimensional low-frequency mode predicted by the dispersion relation (4.115), with a direct numerical solution (Short 1997) for $Q = 50$, $E = 100$, $\gamma = 1.2$ and $f_{OD} = 1.2$. For $k = 0$, both solutions predict the presence of two non-oscillatory modes. For $k > 0$, the asymptotic solution predicts that the growth rate of the smaller mode increases, while that of the larger mode decays. At $k = 0.53$, the two non-oscillatory modes merge into a single propagating oscillatory mode with growth rate $\text{Re}(\lambda) = 0.68$ at $k = 0.53$. The growth rate of this oscillatory mode then increases slightly with increasing k reaching a maximum at $k = 0.76$, before decaying and ultimately stabilizing at $k = 3.17$. Thus stability of the detonation wave is predicted for large wavenumbers, and this feature explains why detonation cells are not observed in very thin channels (Abouseif & Toong 1986; Strehlow 1970). The direct numerical solution closely mimics this behaviour, predicting a merging of the non-oscillatory modes at $k = 0.67$, with stability occurring at $k = 3.05$. We note that in this case, the fastest growing mode is the one-dimensional non-oscillatory mode at $k = 0$.

Figure 7 shows a comparison of the migration of the growth rate $\text{Re}(\lambda)$ and

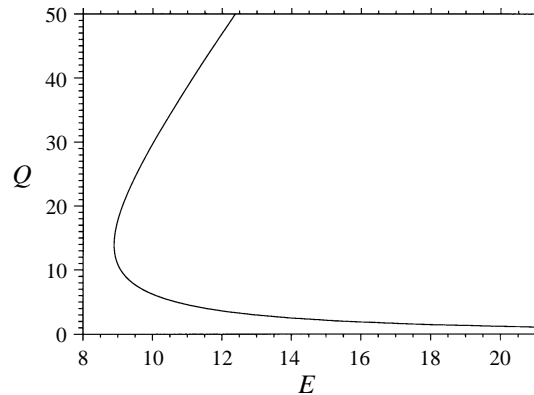


FIGURE 5. The one-dimensional low-frequency neutral stability curve in the (E, Q) -plane with $\gamma = 1.2$ and $f_{OD} = 1$, as calculated from (4.115). The region to the left of the curve corresponds to stability, and to the right, instability.

frequency $\text{Im}(\lambda)$ with wavenumber k for the two-dimensional low-frequency mode predicted by (4.115), with a direct numerical solution for $Q = 50$, $E = 50$, $\gamma = 1.2$ and $f_{OD} = 1$, i.e. with the steady detonation wave running at the Chapman–Jouguet velocity. Figure 7 shows qualitatively similar behaviour to that observed in figure 6. The two non-oscillatory modes present for $k = 0$ in both the asymptotic and numerical solutions merge into a single oscillatory mode at $k = 0.42$ (asymptotic) and $k = 0.29$ (numerical). In both cases the growth rate of the oscillatory mode is observed to increase with increasing k , reaching a maximum at $k = 1.31$ (asymptotic) and $k = 0.82$ (numerical), before decaying and stabilizing at $k = 3.95$ (asymptotic) and $k = 2.77$ (numerical). Thus the dispersion relation (4.115) again predicts that the detonation wave will be stable to disturbances with a sufficiently large wavenumber. Moreover, both solutions select maximum growth rates $\text{Re}(\lambda) = 0.78$ at $k = 1.31$ (asymptotic) and $\text{Re}(\lambda) = 0.55$ at $k = 0.82$ (numerical) when the mode is oscillatory, i.e. for $k > 0.42$ (asymptotic) and for $k > 0.29$ (numerical). However, as seen in figure 6, the fastest growing mode in both cases is the one-dimensional non-oscillatory mode at $k = 0$.

Figure 8 is a plot of the migration of the growth rates and frequencies with wavenumber k of the lowest-frequency modes of instability, as predicted by the dispersion relation (4.115) for $Q = 50$, $E = 50$, $\gamma = 1.2$ and $f_{OD} = 1.5$ (solid lines), $f_{OD} = 2.0$ (dotted lines) and $f_{OD} = 2.5$ (dashed lines). All modes are oscillatory in nature, with the modes corresponding to $f_{OD} = 1.5$ and $f_{OD} = 2.0$ being one-dimensionally unstable, while that corresponding to $f_{OD} = 2.5$ being one-dimensionally stable. For the modes corresponding to $f_{OD} = 1.5$ and $f_{OD} = 2.0$, the growth rates increase with increasing wavenumber k , reaching a maximum $\text{Re}(\lambda) = 0.612$ at $k = 1.53$ ($f_{OD} = 1.5$) and $\text{Re}(\lambda) = 0.490$ at $k = 1.46$ ($f_{OD} = 2.0$). After reaching the maximum, the growth rate of each of these mode decays with increasing k , before stabilizing at $k = 3.90$ ($f_{OD} = 1.5$) and $k = 3.30$ ($f_{OD} = 2.0$). For the one-dimensionally stable mode corresponding to $f_{OD} = 2.5$, the growth rate again increases with increasing wavenumber k and renders the detonation unstable to transverse disturbances when $k > 0.15$. The growth rate then continues to increase with further increases in k , reaching a maximum $\text{Re}(\lambda) = 0.395$ at $k = 1.38$, before decaying and stabilizing at $k = 2.93$. In all cases, the dispersion relation (4.115) selects a maximum growth rate at the critical finite wavenumbers given above. Moreover, since each of these wavenumbers is of or-

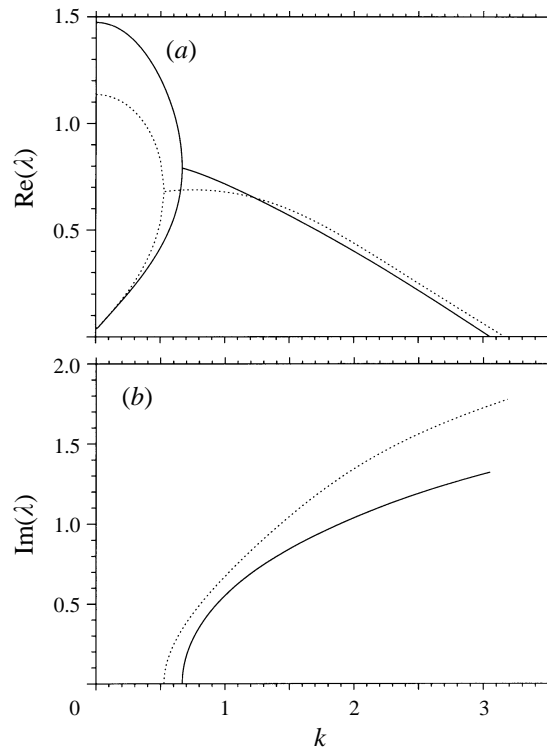


FIGURE 6. The migration of (a) the growth rate $\text{Re}(\lambda)$ and (b) the frequency $\text{Im}(\lambda)$ with wavenumber k of the two-dimensional low-frequency linear disturbance, as calculated numerically in Short (1997) (solid lines) and asymptotically (dotted lines) from (4.115) with $Q = 50$, $E = 100$, $\gamma = 1.2$ and $f_{OD} = 1.2$.

der unity, the corresponding curvature of the detonation front at these wavenumbers would vary on the scale of the induction-zone length.

Figure 9 is a plot of the migration of the growth rates and frequencies with wavenumber k of three low-frequency modes of instability, as predicted by the dispersion relation (4.115) for a Chapman–Jouguet detonation with $Q = 50$, $f_{OD} = 1.0$, $\gamma = 1.2$ and $E = 50$ (solid lines), $E = 20$ (dotted lines) and $E = 10$ (dashed lines). The mode corresponding to $E = 10$ is oscillatory and one-dimensionally stable; the mode corresponding to $E = 20$ is again oscillatory but one-dimensionally unstable; while the mode corresponding to $E = 50$ is that discussed in figure 7, consisting of two non-oscillatory modes at $k = 0$ and a single oscillatory mode for $k > 0.42$. The behaviour of these modes captures all the different characteristic properties associated with two-dimensional linear instability. The mode corresponding to $E = 10$ becomes unstable at $k = 0.16$, reaches a maximum growth rate $\text{Re}(\lambda) = 0.779$ at $k = 2.20$ and stabilizes at $k = 5.06$. The mode corresponding to $E = 20$ has a positive growth rate $\text{Re}(\lambda) = 0.275$ at $k = 0$, reaches a maximum $\text{Re}(\lambda) = 0.897$ at $k = 2.32$, and stabilizes at $k = 5.36$. As above, the mode corresponding to $E = 50$ has two non-oscillatory roots at $k = 0$ with growth rates $\text{Re}(\lambda) = 0.040$ and $\text{Re}(\lambda) = 1.065$. These roots merge into an oscillatory mode at $k = 0.42$, with the oscillatory mode having a maximum growth rate $\text{Re}(\lambda) = 0.78$ at $k = 1.31$, before stabilizing at $k = 3.95$. The wavelengths $W = 2\pi/k$, corresponding to the wavenumbers at which the maximum growth rates occur for $E = 10$ and $E = 20$, are given respectively by $W = 2.86$ and

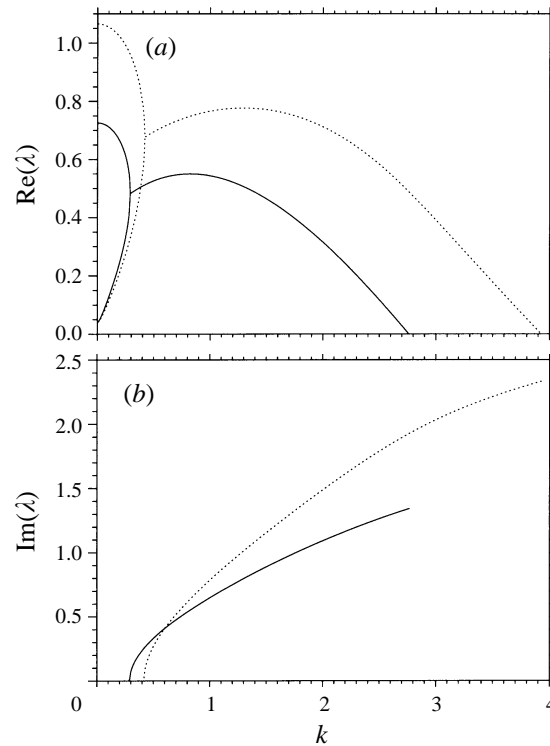


FIGURE 7. The migration of (a) the growth rate $\text{Re}(\lambda)$ and (b) the frequency $\text{Im}(\lambda)$ with wavenumber k of the two-dimensional low-frequency linear disturbance, as calculated numerically in Short (1997) (solid lines) and asymptotically (dotted lines) from (4.115) with $Q = 50$, $E = 50$, $\gamma = 1.2$ and $f_{OD} = 1$.

$W = 2.71$. The wavelength corresponding to the wavenumber at which the growth rate of the oscillatory component of the $E = 50$ mode reaches a maximum is given by $W = 4.80$.

Having determined these critical wavelengths, we now comment on the conjecture made in §1. For a significant range of detonation parameters, it is found that in direct numerical simulations of one-dimensional instability, the nonlinear pulsation frequency corresponds to that of the lowest-frequency linearly unstable mode. We now ask whether an analogy could arise in two-dimensional nonlinear cellular detonation simulations. More specifically, it has been proposed that for a range of detonation parameters, the cell width observed in direct two-dimensional simulations might correspond to the wavenumber associated with the maximum growth rate of the *lowest-frequency* oscillatory mode found in the linear stability analysis. Thus although there might be larger growth rates corresponding to higher-frequency disturbances in the linear stability spectra, it is the lowest-frequency mode which will determine the cell size in the unstable two-dimensional detonation propagation.

In experimental investigations of cellular detonation propagation the following scenario is, however, typically observed (Strehlow 1970). After initiation, small cells emerge initially, but larger cells develop with longer propagation times. These long-time cells are substantially larger than the steady induction-zone length of the detonation. Based on the behaviour of the dispersion relations shown in figures 8 and 9, the wavelengths corresponding to the maximum growth rates identified above could define these initial cell spacings, and would imply that these cells are of the

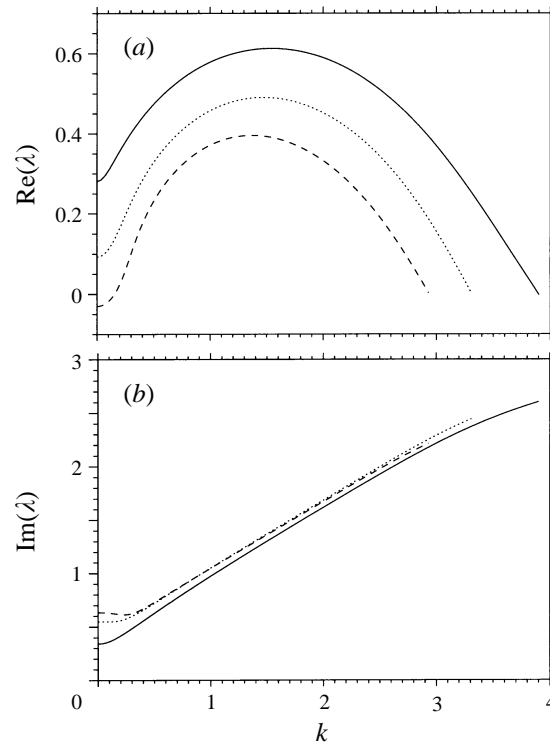


FIGURE 8. The migration of (a) the growth rate $\text{Re}(\lambda)$ and (b) the frequency $\text{Im}(\lambda)$ with wavenumber k of the two-dimensional low-frequency linear disturbances, as calculated asymptotically from (4.115) with $Q = 50$, $E = 50$ and $\gamma = 1.2$ and with $f_{OD} = 1.5$ (solid lines), $f_{OD} = 2.0$ (dotted lines) and $f_{OD} = 2.5$ (dashed lines).

order of the induction-zone length. The selection mechanism for the larger cells which develop for later times then remains to be explained, and given the typical size of these cells, this must be associated with the behaviour of the low-wavenumber dynamics.

Clues for the resolution of this problem can be obtained from the nonlinear evolution equation derived by Yao & Stewart (1996). Numerical solutions of this equation give rise to a unique final cell spacing for parameters where the detonation is stable to one-dimensional disturbances. The cell spacing is found to be determined by the long wavelength associated with the low-frequency neutral stability point where the detonation first becomes unstable to transverse disturbances. For the majority of detonation parameters though, the detonation is unstable to one-dimensional disturbances, and the criteria developed in Yao & Stewart (1996) cannot be used to determine a cell spacing in such cases. The neutral stability point found in Yao & Stewart (1996), however, corresponds to both the points of maximum phase velocity $c_p = \text{Im}(\lambda)/k$ and group velocity $c_g = \partial(\text{Im}(\lambda))/\partial k$ for the linear mode.

Figure 10 shows the corresponding phase and group velocities associated with the dispersion relations for the three modes plotted in figure 9. Only the mode for $E = 10$ has a low-wavenumber neutral stability point. Of most interest is the behaviour of the group velocity c_g . For the mode corresponding to $E = 10$, the group velocity has a maximum $c_g = 0.841$ at $k = 0.288$. For the mode corresponding

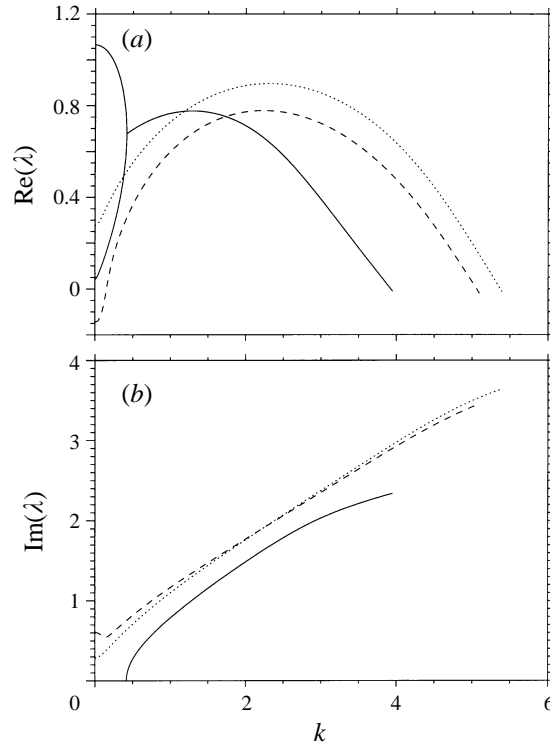


FIGURE 9. The migration of (a) the growth rate $\text{Re}(\lambda)$ and (b) the frequency $\text{Im}(\lambda)$ with wavenumber k of the two-dimensional low-frequency linear disturbances, as calculated asymptotically from (4.115) with $Q = 50$, $f_{OD} = 1$ and $\gamma = 1.2$ and with $E = 50$ (solid lines), $E = 20$ (dotted lines) and $E = 10$ (dashed lines).

to $E = 20$, the group velocity has a maximum $c_g = 0.978$ at $k = 0.232$. For $E = 50$, the group velocity has a maximum $c_g = \infty$ at $k = 0.415$, precisely at the bifurcation point where the two non-oscillatory modes merge into a single oscillatory mode. The wavelengths corresponding to these maximum group velocities are given respectively by $W = 21.82$, $W = 27.08$ and $W = 15.14$, substantially larger than the induction-zone length scaling. Since the energy of the mode is propagated at the group velocity, it is these wavelengths which could determine the final cell spacing observed. However, we emphasize that this is only conjecture based on linear theory, and long-time nonlinear numerical simulations must be carried out in order to verify these statements. The corresponding phase velocities for the three modes shown in figure 9 have maxima $c_p = \infty$ at $k = 0$ for $E = 10$ and $E = 20$, and a maximum $c_p = 0.786$ at $k = 1.038$ for $E = 50$. For the region of instability associated with the mode corresponding to $E = 10$, the phase velocity has a maximum $c_p = 3.3$ at $k = 0.16$, i.e. at the neutral stability point. In summary, we conclude that although the initial cell spacing might correspond to the wavelengths associated with the maximum growth rate of the lowest-frequency linear mode, the long-time evolution is governed by low-wavenumber dynamics, which in turn could be associated with the presence of maxima in the group or phase velocities.

The final diagram, figure 11, is the two-dimensional low-frequency neutral stability curve in activation energy (E)–wavenumber (k) space for $Q = 50$, $\gamma = 1.2$ and for a Chapman–Jouguet detonation with $f_{OD} = 1.0$, as predicted by the dispersion relation

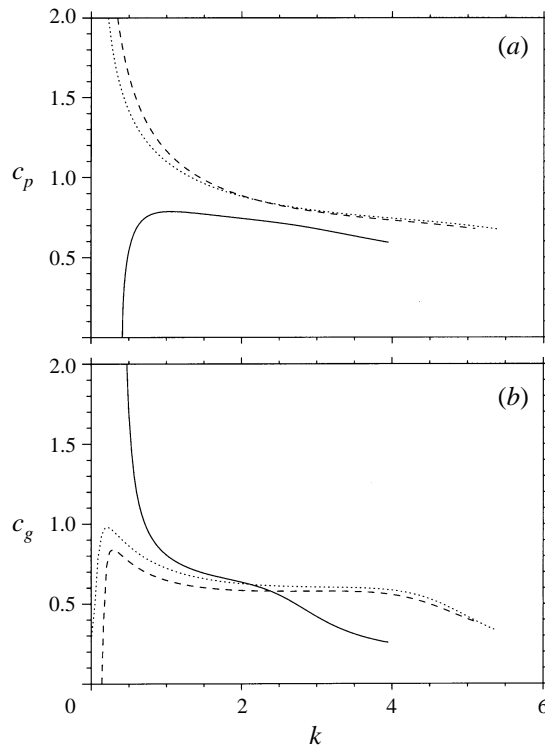


FIGURE 10. The behaviour of (a) the phase velocity $c_p = \text{Im}(\lambda)/k$ and (b) the group velocity $c_g = \partial \text{Im}(\lambda)/\partial k$ with wavenumber k for the three modes shown in figure 9. The solid lines correspond to $E = 50$, the dotted lines to $E = 20$ and the dashed lines to $E = 10$.

(4.115). The region between the two solid lines represents the domain of instability. For $E < 12.4$ the detonation is one-dimensionally stable, but has a band of instability over a finite domain of k , the detonation also being stable for large wavenumbers. For $E > 12.4$ the detonation is one-dimensionally unstable, but also has a finite band of instability in k -space, again due to stability at large wavenumbers. We note that this is typical of the behaviour of two-dimensional perturbations to a detonation wave, and for all activations greater than $E = 5$, the lowest calculated here, the detonation is always two-dimensionally unstable to at least some finite range of transverse wavenumbers.

7. Summary

We have derived an analytical dispersion relation governing the low-frequency two-dimensional linear stability of a plane detonation wave which is travelling either at the Chapman–Jouguet detonation speed or is overdriven. This asymptotic analysis employs the successive limits of high activation energy and the Newtonian limit, in which the ratio of specific heats $\gamma \rightarrow 1$. The dispersion relation retains a dependence on the activation energy, and comparisons with the behaviour of the exact numerical solutions of the low-frequency linear stability spectrum are very favourable. For one-dimensional disturbances, the dispersion relation predicts that stability of the detonation wave is attained for decreasing activation energy (E) or increasing overdrive f_{OD} . For two-dimensional disturbances, the growth rate $\text{Re}(\lambda)$ of

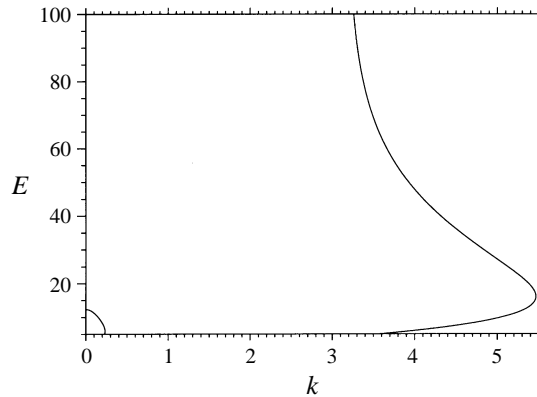


FIGURE 11. The low-frequency two-dimensional neutral stability curve disturbances in (E, k) -space for $Q = 50$, $\gamma = 1.2$ and $f_{OD} = 1$, as calculated from (4.115). The region in between the two curves corresponds to the domain of instability.

each one-dimensional oscillatory low-frequency disturbance is predicted to increase with increasing wavenumber k before reaching a maximum at a finite wavenumber, where typically $k \sim O(1)$. Further increases in k result in a decay in the growth rate of the mode, until a critical wavenumber is reached where typically $k \gg 1$, at which point the mode becomes stable. All these features closely mimic the behaviour of the corresponding numerically evaluated modes.

The mechanisms governing the low-frequency linear instability of detonation waves are highlighted and are shown to involve a complex coupling of acoustic wave disturbances and entropy changes in the induction zone of the detonation. Simplified forms of the dispersion relation and weakly nonlinear evolution equations corresponding to these relations, together with the recovery of the results of Buckmaster & Ludford (1987) when $\lambda \sim O(1/\theta)$, $k \sim O(1/\theta)$, Buckmaster (1989) when $\lambda \sim O(1/\theta)$, $k \sim O(1/\theta^{1/2})$, and Short (1996) when $\lambda \sim O(1)$, $k \sim O(1)$ will be investigated in a future article, where a more detailed mathematical examination of the mechanism governing the linear instability will also be presented.

Finally, we close by suggesting that the results presented here can be improved even further by considering a distinguished limit between the inverse activation energy and $(\gamma - 1)$, where $(\gamma - 1) = O(\theta^{-1})$ (Short 1996). This would have the effect of including the weak $O(\theta^{-1})$ spatially varying steady-detonation structure in the induction zone. This is omitted in the present study due to the nature of the ordered limit we have considered, and should lead to better quantitative, if not qualitative, agreements.

M.S. was supported by the US Air Force Office of Scientific Research, Mathematics (F49620-96-1-0260) and by the Engineering and Physical Sciences Research Council (UK). D.S.S. was supported by US Air Force Wright Laboratories, Armament Directorate (F08630-94-10004) and the US Air Force Office of Scientific Research, Mathematics (F49620-93-1-0532). The authors are grateful for the criticisms and suggestions made by the three referees which lead to an improved manuscript. M.S. is also grateful for discussions with Professor J. F. Clarke on properties of the two-dimensional generalization of the nonlinear Clarke's equations (Clarke 1981) in a mean flow.

REFERENCES

- ABOUSEIF, G. & TOONG, T. Y. 1982 Theory of unstable one-dimensional detonations. *Combust. Flame* **45**, 64–94.
- ABOUSEIF, G. & TOONG, T. Y. 1986 Theory of unstable two-dimensional detonations: Genesis of the transverse waves. *Combust. Flame* **63**, 191–207.
- ALPERT, R. L. & TOONG, T. Y. 1972 Periodicity in exothermic hypersonic flows about blunt projectiles. *Astron. Acta* **17**, 539–560.
- BLYTHE, P. A. & CRIGHTON, D. G. 1989 Shock generated ignition: the induction zone. *Proc. R. Soc. Lond. A* **426**, 189–209.
- BOURLIOUX, A. & MAJDA, A. J. 1992 Theoretical and numerical structure for unstable two-dimensional detonations. *Combust. Flame* **90**, 211–229.
- BOURLIOUX, A., MAJDA, A. J. & ROYTBURD, V. 1991 Theoretical and numerical structure for unstable one-dimensional detonations. *SIAM J. Appl. Maths* **51**, 303–343.
- BUCKMASTER, J. D. 1988 Pressure transients and the genesis of transverse shocks in unstable detonations. *Combust. Sci. Tech.* **61**, 1–20.
- BUCKMASTER, J. D. 1989 A theory for triple point spacing in overdriven detonation waves. *Combust. Flame* **77**, 219–228.
- BUCKMASTER, J. D. & LUDFORD, G. S. S. 1987 The effect of structure on the stability of detonations I. Role of the induction zone. In *Twenty-first Symp. (Intl) on Combustion*, pp. 1669–1676. The Combustion Institute.
- BUCKMASTER, J. D. & NEVES, J. 1988 One-dimensional detonation stability: The spectrum for infinite activation energy. *Phys. Fluids* **31**, 3571–3576.
- CLARKE, J. F. 1981 Propagation of gas-dynamic disturbances in an explosive atmosphere. *Prog. Astro. Aero.* **76**, 383–402.
- ERPENBECK, J. J. 1963 Structure and stability of the square-wave detonation. In *Ninth Symp. (Intl) on Combustion*, pp. 442–453. The Combustion Institute.
- ERPENBECK, J. J. 1964 Stability of idealized one-reaction detonations. *Phys. Fluids* **7**, 684–696.
- FICKETT, W. & WOOD, W. W. 1966 Flow calculations for pulsating one-dimensional detonations. *Phys. Fluids* **9**, 903–916.
- LEE, H. I. & STEWART, D. S. 1990 Calculation of linear instability: one-dimensional instability of plane detonation. *J. Fluid Mech.* **216**, 103–132.
- NAYFEH, A. N. 1973 *Perturbation Methods*. John Wiley & Sons.
- QUIRK, J. J. 1994 Godunov-type schemes applied to detonation flows. In *Combustion in High-Speed Flows* (ed. J. Buckmaster, T. L. Jackson & A. Kumar), pp. 575–596.
- QUIRK, J. J. 1995 A parallel adaptive mesh refinement algorithm for computational shock hydrodynamics. *Appl. Numer. Maths* **20**, 427–453.
- SHORT, M. 1996 An asymptotic derivation of the linear stability of the square wave detonation using the Newtonian limit. *Proc. R. Soc. Lond. A* **452**, 2203–2224.
- SHORT, M. 1997 Multi-dimensional linear stability of a detonation wave at high-activation energy. *SIAM J. Appl. Maths* **57**, 306–326.
- STEWART, D. S., ASLAM, T. D. & YAO, J. 1996 On the evolution of cellular detonation. In *Twenty-sixth Symp. (Intl) on Combustion*. The Combustion Institute (in press).
- STREHLOW, R. A. 1970 Multi-dimensional detonation wave structure. *Astron. Acta* **15**, 345–357.
- YAO, J. & STEWART, D. S. 1996 On the dynamics of multi-dimensional detonation waves. *J. Fluid Mech.* **309**, 225–275.
- ZAIDEL, R. M. 1961 The stability of detonation waves in gaseous detonations. *Dokl. Akad. Nauk SSSR (Phys. Chem. Sect.)* **136**, 1142–1145.